The Impact of Stromal Cells on the Metabolism of Ovarian Cancer Cells in 3D Culture

Emily Seton Pyne

Thesis submitted to the faculty of Virginia Polytechnic Institute and State University in partial fulfillment of the requirements for the degree of

Master of Science
In
Human Nutrition, Foods and Exercise

Eva M. Schmelz, Chair
Madlyn I. Frisard
Benjamin A. Corl

Tuesday December 6th, 2016
ILSB 1040
Blacksburg, Virginia

The Impact of Stromal Cells on the Metabolism of Ovarian Cancer Cells in 3D Culture

Emily Seton Pyne

ACADEMIC ABSTRACT

Ovarian cancer is the leading cause of death among female gynecologic cancers. Current treatments include surgical debulking, and chemotherapy. However, better interventions are needed to reduce the mortality rate of metastatic disease. Ovarian cancer cells have displayed the ability to aggregate and form 3D homogeneous and heterogeneous spheroids, which can function as micrometastases. Ovarian cancer spheroids survive independently prior to adhering to an endothelial tissue. Since aggregation has been shown to provide a survival advantage to the spheroids and increased their aggressive phenotype, this study aimed to investigate how the metabolism of ovarian cancer cells change in 3-dimensional (3D) culture. Examining metabolic pathways and identifying markers of metabolic change could provide the scientific base for new, targeted interventions for this disease. Spheroids of both homogeneous and heterogeneous composition demonstrated overall lower metabolic capacity than their adherent counterparts. Spheroids had a lower basal energetic demand than adherent cells, paralleled by lower maximal respiration capacity, glycolytic capacity, and spare respiratory capacity. We conclude that the lower energetic demand of spheroids may be a mechanism to prolong death by reserving energy and metabolic cellular processes; this may render anti-metabolic drug treatment with AICAR or metformin ineffective against disseminating ovarian cancer aggregates.

The Impact of Stromal Cells on the Metabolism of Ovarian Cancer Cells in 3D Culture

Emily Seton Pyne

GENERAL ABSTRACT

Ovarian cancer is currently the leading cause of death among female gynecologic cancers. While treatments exist, better interventions are needed to reduce the mortality rate in this form of cancer. Ovarian cancer cells have displayed the ability to aggregate and form 3D homogeneous and heterogeneous spheroids, which can function as micrometastases. Ovarian cancer spheroids survive independently prior to adhering to an endothelial tissue. Since aggregation has been shown to provide a survival advantage to the spheroids and increased their aggressive phenotype, this study aims to investigate how the metabolism of ovarian cancer cells change in 3-dimensional (3D) culture. Examining metabolic pathways and identifying markers of metabolic change could provide the scientific base for new, targeted interventions for this disease.

ACKNOWLEDGEMENTS

Eva, it is hard to figure out where to begin thanking you. Simply put, I would not have made it through this degree without you. I will be forever grateful for your kindness and in admiration of your brilliance. You challenged me to be an independent thinker and an autonomous worker, but I could always count on you for counsel when needed. I am inspired by your scientific endeavors and your incredible strength as an individual. You have me made a better scientist and expanded my knowledge infinitely. Your guidance and friendship are invaluable, and I feel truly blessed to have had you as my mentor. You are an irreplaceable figure in my life, thank you for everything.

Madlyn, thank you so much for being the person that saw the potential for a master's candidate in me. From the beginning you encouraged me to pursue this degree and guided me through many challenges along the way. I am so grateful for this opportunity and your mentorship.

Lu and Jack, I could not have asked for better lab colleagues. I am so proud of the teamwork that we demonstrated and am thankful for having people that I could discuss ideas with, rely on for help, and that I genuinely enjoyed working with.

You both made this experience the positive and fun journey that it was. I wish you both the best of luck in your future endeavors.

Mom and Dad, it would not have been possible for me to complete this work without your support. Through many ups and downs, academic and otherwise, you never faltered, and gave me perspective and comfort at the moments that I needed them most. You've been my biggest cheerleaders, my shoulders to cry on, and my ears to vent to. Your encouragement has truly been vital to my ability to finish and I can't possibly thank you enough for everything you've done to get me to this point. I love you both so much.

Table of Contents

I. INTRODUCTION

Cancer is a family of diseases affecting metazoans that results from an accumulation of genomic alterations. Cells of this disease are all marked by characteristics such as sustained, self-sufficient growth and evasion of apoptosis. In order to support this high rate of reproduction, cancer cells exhibit the ability to deregulate normal energetic processes. This also allows them to survive in environments where non-transformed cells could not. Otto Warburg first identified this phenomenon and located its origin: a glycolytic shift, dubbed "the Warburg Effect" for its discoverer. Warburg observed that cancer cells increase glycolysis and eliminate the excess carbons in the form of lactate.

In the case of ovarian cancer, studies have begun to identify the time at which metabolic shifts occur in the progression of the disease. However, most of the metabolic changes identified occurred in late stage cells meaning that they would not serve as a marker of early stage cancer, and thus are not a good method of early detection. In addition, ovarian cancer is usually diagnosed in later stages, which significantly affects prognosis. Therefore it would be advantageous to identify novel metabolic targets during the progression of the disease for better treatments.

Previous studies on the metabolism of ovarian cancer were also largely conducted in adherent monolayer environments which fail to address one of the unique aspects of ovarian cancer: its method of dissemination throughout the peritoneal cavity. Initially, cells are exfoliated from the ovaries and spread into the peritoneal cavity, facilitating their spread to other areas of the body. These cancer cells can aggregate and form homogeneous or heterogeneous multicellular spheroids. Spheroids can further spread throughout the abdomen via peritoneal serous fluid flow and eventually attach to tissues to initiate metastatic outgrowths.

The goal of this project is to investigate the metabolism of ovarian cancer cells, specifically during the aggregation into both homogeneous and heterogeneous spheroids. We hypothesize that an altered metabolism may contribute to the increased metastatic potential, survival, and aggressive outgrowth observed in spheroids. A better understanding of the bioenergetics of ovarian cancer spheroids could identify novel targets for treatment for metastatic ovarian cancer.

II: REVIEW OF LITERATURE

Background

Ovarian cancer is diagnosed in about 20,000 women in the United States each year and causes more deaths than any other cancer of the female reproductive system. Treatments can be effective when the disease is detected in early stages. However, there currently is a lack of effective early detection methods. Thus, this cancer is generally found at later stages. As expected, later detection contributes to a low survival rate past 5 years in remission, at less than 50 percent.[1,2] Furthermore, the current standard of treatment is largely restricted to surgery and chemotherapy, both of which are either invasive or toxic with the potential for further harm and complications.[3] Ovarian cancer is very heterogeneous in genetics, histology, and origin. The most common form, serous ovarian cancer, originates in the surface epithelium of the ovaries or fallopian tubes. It is also the most deadly form of the disease.[4,5]

One possible barrier to both early detection and more effective treatments for this disease is the altered metabolic phenotype seen in cancer cells, which makes them adaptive in a dynamic microenvironment and, thus, better able to survive changing conditions. This phenomenon is now included in the hallmarks of cancer, generally referred to as "deregulation of cellular energetics". One form of energetic deregulation in cancer cells is known as the "Warburg effect", labeled as such for its discovery by Otto Warburg, who observed a glycolytic shift in cancer cells. He found an increase in glucose uptake as well as lactate secretion and production in the cancer cells. He concluded that cancer cells must have impaired mitochondria and use aerobic glycolysis as the primary source of ATP synthesis, rather than oxidative phosphorylation.[6,7] However, later research found that most tumor cells with fully functional mitochondria can still exhibit the Warburg effect, indicating that the impaired mitochondria

hypothesis may not hold true in all cancers.[8] Sidney Weinhouse proposed that the increase in lactate excretion occurred simply because the glycolytic flux is too high to sustain oxidative phosphorylation.[9] Since Weinhouse first postulated that mitochondria are not impaired in cancer cells, subsequent research has confirmed his theory.[10,11]

In order to study metabolic changes that occur during the progression of ovarian cancer, this project uses cell lines that model the stages of the disease. By using serial passaging of primary murine ovarian surface epithelial cells to induce spontaneous immortalization and transformation, a line of genetically and phenotypically distinct ovarian cancer cells were captured. This model, known as the mouse ovarian surface epithelial (MOSE) cell model, has been thoroughly characterized at early, intermediate, and late stages, representing a spectrum of the disease from benign to highly aggressive. A model such as this does not exist for the human disease and is valuable for comparing stages of the disease to understand how it progresses. These cells exhibit increased growth rate and the ability to form spheroids as they progress. Such changes in the cells are accompanied by changes in gene expression and dysregulation of cellular architecture.[12,13] The tumorigenic late stage cells (MOSE-L) have changes in substrate utilization and mitochondrial function as compared to the early and intermediate stages (Figure 1).[14]

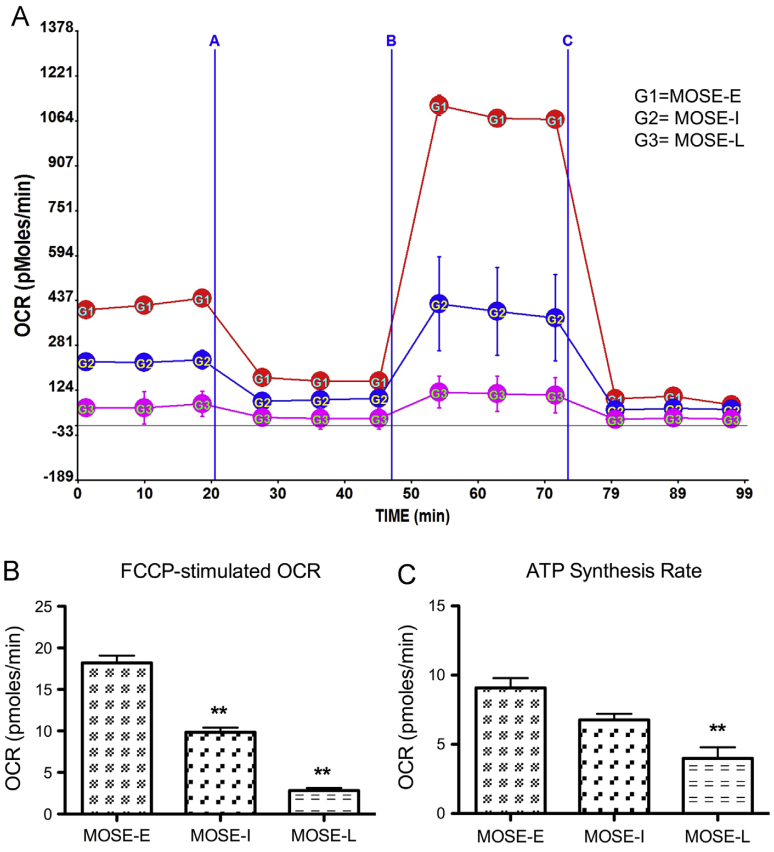

Figure 1. Oxidative Capacity Rate is reduced in a step-wise manner during MOSE cell progression. (A) Image of representative experiment where A is oligomycin treatment, B is FCCP treatment and C is rotenone treatment, measured over approx. 2 h; (B) Change over base-line in oxygen consumption rate (OCR) after FCCP treatment, which causes uncoupling of mitochondria; (C) ATP synthesis rate as calculated by the difference between basal OCR and oligomycin-blocked OCR. The MOSE model progression is accompanied by changes in mitochondrial function as seen by changes in oxygen consumption rate. Image from Anderson et al.[14]

To further investigate the high rate of relapse that occurs in ovarian cancer after initial debulking surgery and chemotherapy, this study uses a variant cell population derived from the MOSE-L cells by in vivo passaging with tumor-initiating properties (TICs).[15] In cancer, TICs within a tissue are distinctly different from the benign and malignant cell population in a tissue and exhibit a unique phenotype.[16,17] Importantly, it has been found that platinum-resistant ovarian tumors often harbor populations of these TICs or other stem cells. This suggests that TICs may be responsible, at least in part, for recurrent forms of the disease. [18] By using *in vivo* passaging of MOSE-L cells they were enriched for tumor-initiating cells and harvested from ascites to produce a cell culture line of highly aggressive TIC variants with increased tumorigenicity, referred to hereafter as MOSE-L_{TICv} (murine ovarian surface epithelial-late tumor-initiating cell variant). These variants require only 10^4 cells to induce lethal disease in 23 days, where as their parent population of MOSE-L cells need 1-5 x 10^6 cells implanted in a

mouse to induce death, taking 8-10 weeks. The MOSE-L_{TICv}s therefore model fast-developing disease.

A previous study characterized the metabolic phenotype of the MOSE-L_{TICv}s and found that indeed in parallel with the increased growth rate and invasive nature of these cells, they also exhibited a phenotypically distinct metabolic profile compared to the MOSE-L cells they were derived from (Figure 2). The MOSE-L_{TICv}s were more glycolytic than both MOSE-E and MOSE-L cells and also demonstrated a higher maximal respiration when uncoupled, indicating an overall more flexible metabolism compared to the MOSE-L cells which strictly exhibit the classic Warburg effect.[19]

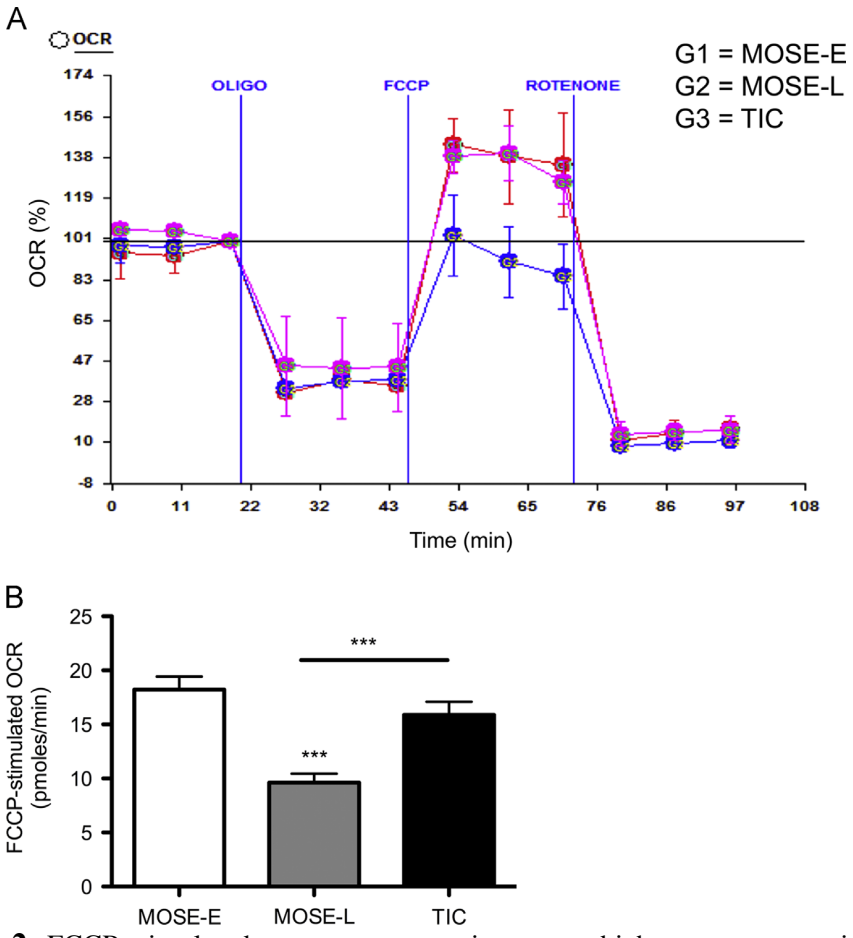

Figure 2. FCCP-stimulated oxygen consumption rate, which represents maximal respiration of

the uncoupled mitochondria, is increased in the TICs. Maximal respiration was measured following administration of carbonylcyanide-p-trifluoromethoxyphenyl hydrazone (FCCP). (A) Image of a representative experiment measured over 2 h with normalization to baseline; and (B) change over baseline in OCR after FCCP treatment. The TICs have a maximal respiration comparable to the early cells and significantly higher than the lates. Image from Anderson et al.[19]

The MOSE-L_{TICv} cells also exhibit the ability to form spheroids in non-adherent culture conditions. In ovarian cancer, spheroids are the result of cellular exfoliation into the peritoneal cavity where cells aggregate and eventually attach to tissues, initiating metastasis. In other cancers, dissemination is often hematogeneous or lymphogeneous. In ovarian cancer, however, cells can spread via the bulk flow of peritoneal serous fluid, which, importantly, can also serve as a reservoir for cells and molecules that promote growth, angiogenesis, adhesion, and invasion.[4,20] The stromal cells in the ascites are often components of the stromal vascular fraction of white adipose tissue, recruited into the peritoneal cavity by tumor or other cells using chemoattractants.[21,22] Thus, these homogeneous or heterogeneous spheroids essentially function as micrometastases and they have also demonstrated increased rates of survival.[23]

The MOSE model also expresses many fallopian markers commonly found on the epithelium such as N-cadherin and the Mullerian inhibitory substance receptor II (MISRII). This indicates that it can serve as a model for the most deadly form of the disease, serous ovarian cancer, which is thought to originate on the epithelium of the fallopian tubes in many cases.[4,5] Given that spheroids play a crucial role in the progression of ovarian cancer, understanding more about serous ovarian carcinoma spheroids and how they survive is critical for developing improved treatments. This project aims to examine the metabolic nature of homogeneous and heterogeneous ovarian cancer spheroids comprised of MOSE-L_{TICv}s and stromal cells to identify potential targets for treatment.

Ovarian cancer spheroids

One of the main challenges that exists in treating ovarian cancer is that the current chemotherapeutic regimens often produce positive initial results but are unable to achieve sustained remission. This is largely attributed to the unique dissemination of cells where they locally invade pelvic and abdominal organs, rather than traveling through vasculature or the lymph.[25] The malignant cells that are shed from the ovaries often aggregate and form spheroid-like structures which are proving to be better able to survive independent of a tissue, to initiate metastasis, and to resist chemotherapeutic treatments.[26-28] This process is outlined in figure 3, where primary cells can be seen exfoliating from the ovary and aggregating, and eventually attaching to secondary sites.

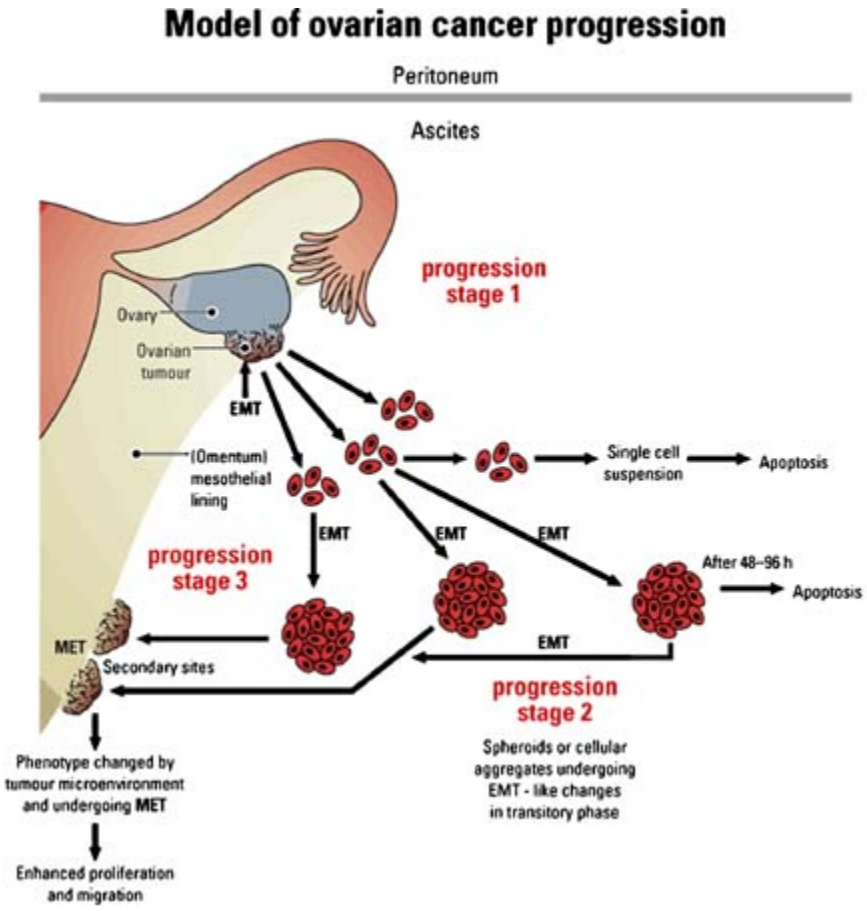

Figure 3. Progression of epithelial ovarian cancer. Ovarian epithelial cells become malignant, form primary tumors on the ovaries, and undergo the epithelial-mesenchymal transition. Through exfoliation

processes, cells are sloughed off into the ascites fluid where they can aggregate and eventually engraft onto the surface of local organs in the pelvic area and abdomen. This process is impacted by numerous microenvironmental regulators. Image from Ahmed et al.[29]

The current standard of treatment for ovarian cancer is cytoreductive surgery followed by chemotherapy, most often a combination of a platinum-based chemotherapy, such as cisplatin or carboplatin, with a taxane, such as paclitaxel or docetaxel.[30,31] This regimen involves systemic administration to the patient. Given that these compounds target key steps in cell division, other proliferating cell populations in the body are affected as well. This treatment can elicit a significant response rate in most patients but recurrence of the disease is very common. It is thought that small pockets of malignant cells, or perhaps spheroids, may be the cause of recurrent disease. If spheroids are capable of protecting cells from chemotherapeutic compounds or other causes of cell death, it is of paramount importance to understand how they achieve this. It is expected that an altered regulation of energetics would contribute to the spheroids ability to evade death and could provide insight into ways to target spheroids, with the hope of reducing rates of recurrent disease.

Ovarian cancer mitochondria

Contrary to the original conclusions of Warburg, ovarian cancer mitochondria work properly. The Krebs cycle and the electron transport chain are both fully functional, which is important to consider given the observation that a glycolytic shift still occurs. In fact, in studies where ovarian cancer tissue was perfused and levels of oxygen consumption and lactate were measured, as much as 90 percent of ATP needs were generated by oxidative phosphorylation.[32,33] Furthermore, in mitochondria isolated from human ovarian cancer tissues the specific activities of key mitochondrial enzymes, mitochondrial membrane potential, ATP biosynthesis, and oxygen consumption rate were all found to be comparable to isolated mitochondria from mouse livers.[34]

However, there are differences in mitochondria of ovarian cancer cells versus normal cells and these differences may lead to important knowledge about the metabolism of ovarian cancer cells. For example, some studies suggest that there is an increased accumulation of ROS (reactive oxygen species) due to a higher membrane potential observed in mitochondria of ovarian cancer cells.[35] This accumulation can enhance the progression of ovarian cancer.[36] ROS has been shown to degrade MAP kinase phosphatase 3 which in turn leads to a constitutively active ERK 1/2 signaling. This is alarming because the ERK signaling pathway has been shown to support tumor progression.[36] Additionally, a study on cisplatin-resistant ovarian cancer cells (cisplatin being a commonly used chemotherapeutic agent) found altered morphology in the mitochondrial cristae, and in some mitochondria no cristae were present at all.[37] The absence of proper cristae formation can actually cause an increase in ROS, membrane potential, and metabolic flux.[38] This observation may prove to be a further reason explaining ROS accumulation and potentiation of the disease.

Specifically in the MOSE model, our lab has demonstrated that there are changes in organization of the mitochondria and in membrane potential.[19] In Figure 3, MOSE-E, MOSE-L, and TIC cells (MOSE-L_{TICv}) were stained with JC-1 to visualize mitochondria membrane potential. The early cells exhibit a more organized network of mitochondria throughout the cell whereas in the MOSE-L and MOSE-L_{TICv} the mitochondria appear rounder and less organized. Furthermore, the mitochondrial membrane potential, which is associated with the capacity of cells to generate ATP, appeared different in the early, late, and TIC cell populations. Hyperpolarized mitochondria were visible in MOSE-E, but only at about 10% in MOSE-L and none in the MOSE-L_{TICv}. However, given that hydrogen peroxide can quench JC-1 emission, mitosox staining was used to visualize superoxides living in each population and indeed there

was a high intensity (the highest of the 3) found in the MOSE-L_{TICv}.[39] This indicates that the lack of JC-1 emission in the TICs may be due to quenching of the dye by reactive oxygen species rather than a depolarized mitochondrial membrane. This was confirmed by staining with mitotracker Green and TMRE, both of which label active mitochondria regardless of membrane potential and are not sensitive to hydrogen peroxide quenching. Flow cytometric analyses indeed revealed that the MOSE-L and TICs have active, highly polarized mitochondria (Figure 4B).[19]

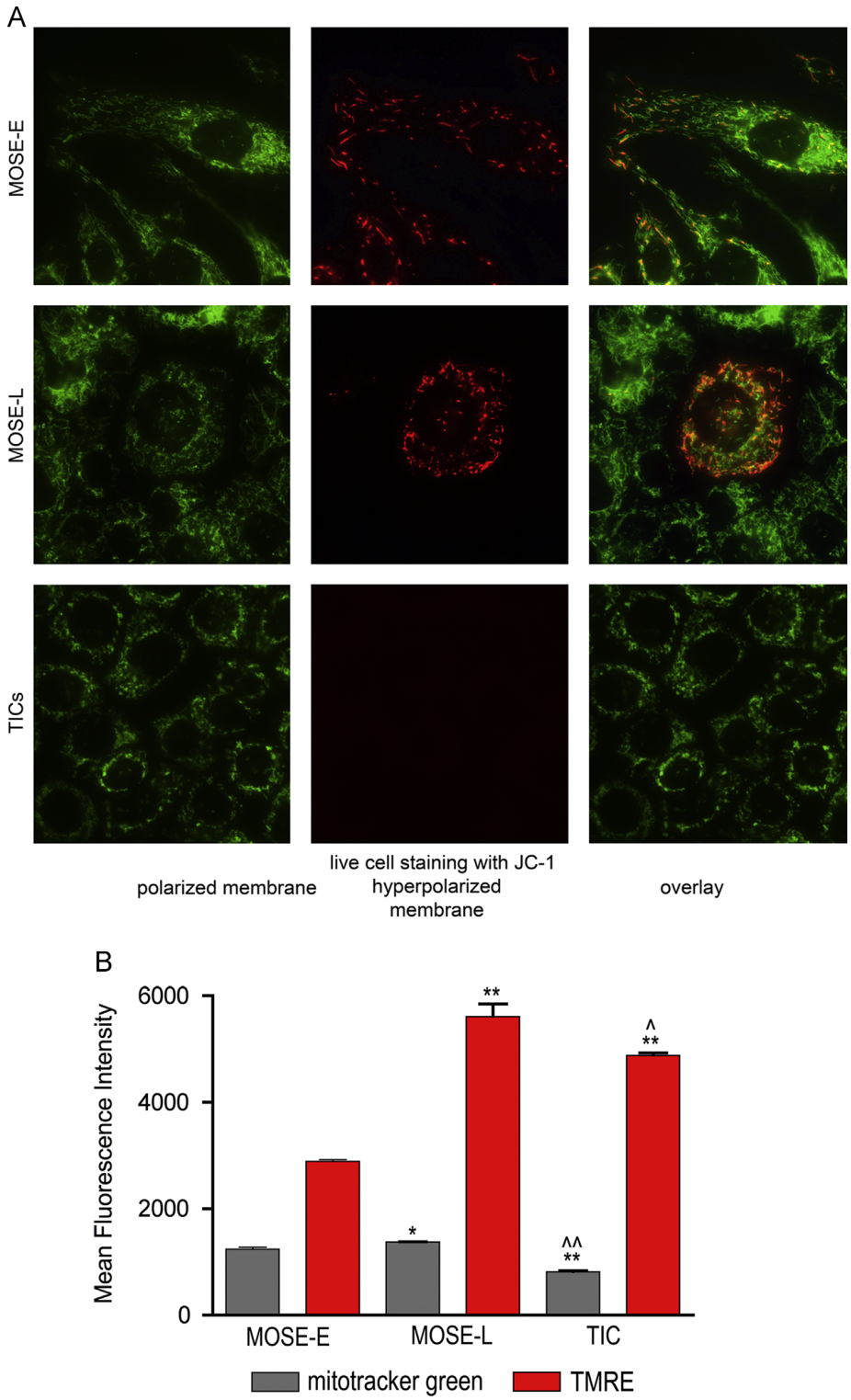

Figure 4. Changes in mitochondria organization and membrane potential among MOSE-E, MOSE-L, and TICs. (A) Live-cell staining of cells with fluorescent mitochondria-specific dyes showing mitochondria organization and membrane hyperpolarization. (B) Changes in geometric mean fluorescence after mitotracker green and TMRE staining. MOSE-L and MOSE-L_{TICv} have viable, polarized mitochondria. Image from Anderson et al.[19]

Another notable observation regarding the MOSE-L_{TICv} mitochondria is their apparent ability to transfer these organelles from cell to cell. In figure 5 mitotracker red staining reveals mitochondria that are in between cells rather than in the cytoplasmic networks surrounding the nuclei. It is unclear which direction the mitochondria are traveling. However, in a study conducted in pheochromocytoma cells, researchers found that mitochondria could be passed from healthy cells to damaged cells via tunneling nanotubes (TNTs). Cells were damaged with UV light and then co-cultured with untreated cells. The untreated cells rescued the UV-treated cells, and a unique type of TNT formed between the damaaged and untreated cells. This type of TNT was characterized by continuous microtubules localized within and, interestingly, mitochondria colocalized with the microbtubules inside the TNTs and moved along them from healthy to damaged cells.[40] The concept of nanotubular highways used for organelle transport among cells has been established, but this insight into a rescue mechanism, using mitochondria, for apoptotic cells may be a key factor in understanding how certain cancer cells evade death. Indeed it appears that it may be occurring in the MOSE-L_{TICv}s, and they at least have the capacity for intracellular mitochondrial transport.[41]

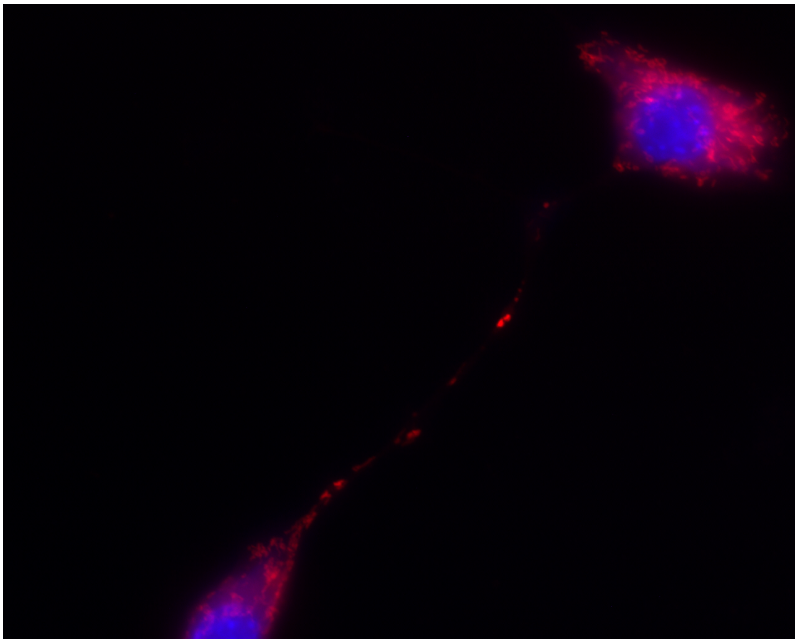

Figure 5. Adherent MOSE-L_{TICv}s stained with Mitrotracker Red CMXROS and DAPI, a nuclear stain. Between two cells there are mitochondria being transferred along what is thought to be a nanotube.

There is limited understanding of the role that mitochondria play in the survival of ovarian cancer spheroids. While some research has investigated parameters such as oxygen consumption rate and extracellular acidification rate in ovarian cancer cell lines, few studies to date have done these measurements in intact spheroids. [25,42] It is important to consider the dynamic interactions that may occur among the mitochondrial network in a 3D environment versus an adherent one, especially given the unique understanding of mitochondria in cancer cells.

Ovarian cancer cells and interactions with other cell types

The conventional understanding of the Warburg effect, that cancer cells exhibit a glycolytic shift, fails to acknowledge the cross-talk that occurs between cancer cells and the other cell populations in their surrounding environment. Recent evidence has highlighted the importance of the cellular heterogeneity of tumor microenvironments specifically in regards to the ways that the microenvironment can supply energy metabolites and chemical building blocks

needed for sustained growth and proliferation. “Tumor microenvironment” refers to all of the non-transformed components of a tumor including blood vessels, adipocytes, fibroblasts, immune cells, and the extracellular matrix.[43] The evolution of the understanding of the tumor microenvironment is depicted in figure 6 where ultimately the theory is that cancer is a complex array of interactions among many cell types; targeting those rather than focus on just cancer cells may be a superior strategy to suppress cancer-related deaths. We see that a tumor is not comprised of only cancer cells, but of a diverse population of other cell types. Thus, understanding only the ways that cancer cells behave is null because their behavior is likely affected by interactions with all the other surrounding cells.

A

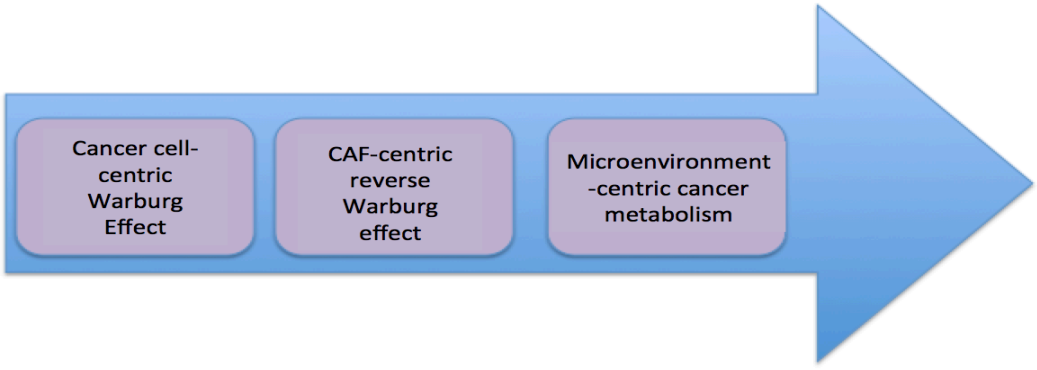

B

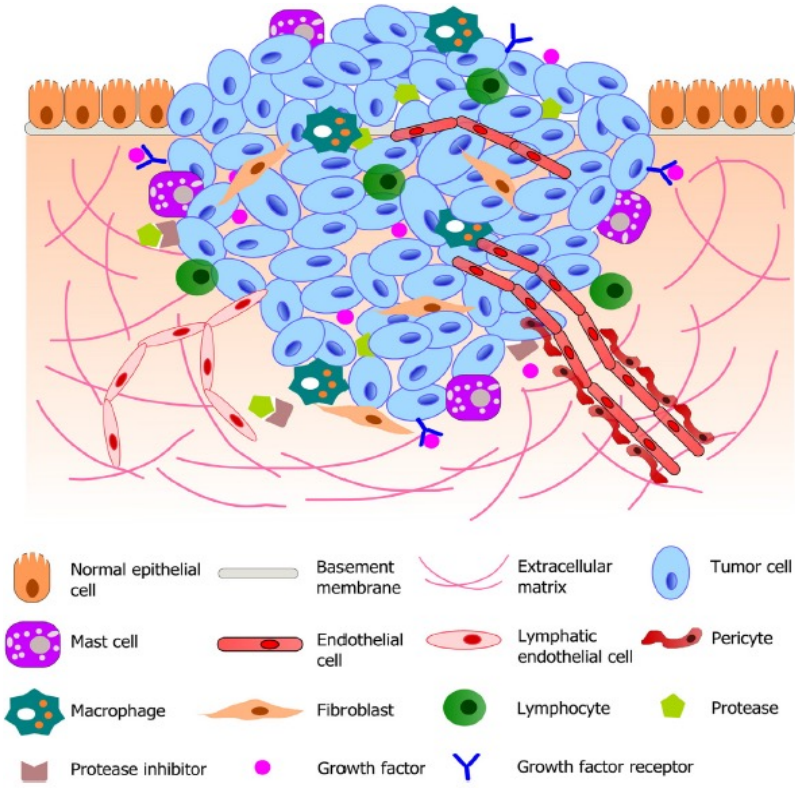

Figure 6. (A) Representation of the shift in hypotheses surrounding the Warburg effect and cancer cell metabolism. Starting with the traditional view of cancer cell-only, it evolved to include dynamic interplay between a variety of components in the tumor microenvironment..[44] (B) A depiction of the tumor microenvironment, demonstrating the potential for a diverse cell population to constitute one tumor. Adapted from Joyce and Pollard, 2009; Koontongkaew, 2013. [45,46]

Endothelial Cells

A critical source of survival for tumors is their blood supply, generated by angiogenesis.[47] Endothelial cells and their progenitor cells are thought to play a role in initiating this process. One of the main tumor-promoting mechanisms of endothelial cells is their ability to provide nutrients and oxygen for tumor growth through neo-angiogenesis.[48] Given that spheroids serve as precursors to tumors in many cases, colonizing the sites where metastasis occurs, it would be helpful to understand if they too benefit from interactions with endothelial cells found in the peritoneal cavity prior to tissue attachment. It is expected that with neo-angiogenic signaling already occurring, the rate of successful invasion would be increased.

Fibroblasts

Fibroblasts in the context of a tumor are known as "cancer-associated fibroblasts", or CAFs. Generally, they are the most abundant subpopulation of cells residing within a tumor microenvironment in most forms of cancer. They have the ability to promote numerous, critical tumorigenic processes such as cell proliferation, angiogenesis, inflammation, and metastasis.[43] In ovarian cancer, the majority of CAFs are likely derived from resident fibroblasts rather than from differentiation and transition of endothelial and epithelial cells.[49] Ovarian cancer cells secrete signaling compounds that activate a phenotypic switch in the fibroblasts from quiescent to activated, or to "CAF".[50] Secretory factors from activated CAFs, including extracellular matrix (ECM) molecules and ECM-modifying enzymes, alter the ECM and likely contribute to changes in rigidness; this is important for the ability to form spheroids.[51] Less is known about the metabolic phenotype of fibroblasts and CAFs, especially in the context of spheroids.

Stromal vascular fraction

With a growing interest in the relationship between obesity and cancer, researchers have started to examine the relationship on a molecular level. Aside from the role that adipocytes play in providing fuel to cancer cells, the stromal vascular fraction (SVF) is emerging as an important factor as well. The SVF is the "junk" of adipose tissue, comprised of various cells in the adipose tissue that are not adipocytes, including endothelial cells, adipocyte progenitors (APCs), immune cells, fibroblasts, pericytes, hematopoietic progenitor/stem cells (HSCs) and mesenchymal stem cells (MSCs).[52,53] Recent studies demonstrated that SVF are able to provide a growth advantage to tumors.[22] This leads to the question of whether they also provide an advantage to spheroids. In Figure 7 it is evident that indeed SVF increases the aggressiveness of MOSE-L_{TICv} cells (shown as MOSE-L FFL in image) when invading collagen. As expected, this also leads to increased proliferation and metastatic potential when the cells are combined.[15,54] In figure 7, cancer cells

(in green) are combined with SVF cells and the resulting spheroid exhibits significant protrusions on the edges. In the overlay image (4th panel on top), the SVF are shown being carried into the protrusions with the cancer cells, suggesting that perhaps the spheroid uses endothelial cells, stem cells, or other precursors to metastasize.[55] These protrusions also appear with the addition of MS1 (endothelial) cells (bottom panel C).

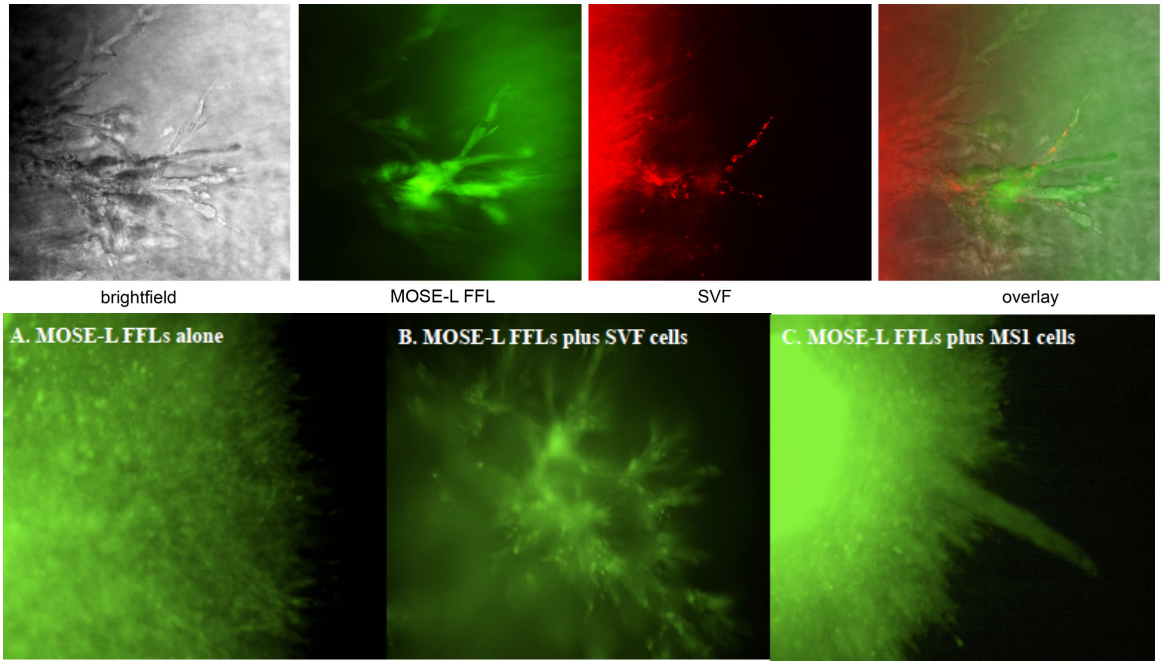

Figure 7. Top: images of outgrowths from MOSE-L FFL and SVF co-cultured spheroids. Bottom: Fluorescent images of MOSE-L FFL outgrowth when cultured A) alone, B) with SVF cells, or C) with MS1 cells.[55] Metastatic outgrowths are visible with the addition of SVF or MS1 cells. Images from Shea dissertation.

Conclusion and Aims

Ovarian cancer continues to be a deadly threat for the thousands of women diagnosed with the disease each year. There is hope for increasing survival rates and reducing rates of recurrent disease by gaining a better understanding of the role homogeneous and heterogeneous spheroids play in the progression of the disease. A glycolytic shift is indeed a hallmark change seen in cancer cells, including ovarian cancer. However, it is not due to dysfunctional mitochondria as

was once thought. While the mitochondria may be different, they are highly functional and may still be an important contributor to the survival of malignant cells and/or to tumor-initiating cells. With preliminary studies providing an understanding of the metabolic changes that accompany the progression of ovarian cancer in adherent cultures, more work is needed to understand the changes following cancer cell dissemination and formation of spheroids, and to understand the role of mitochondrial bioenergetics in metastasis. Further, cancer cells recruit the help of other cell types, and this is a crucial aspect of their ability to survive. Through a better understanding of those interactions, especially in the context of spheroids, novel targets for treatment may be identified that decrease spheroids' ability to survive and cause recurrent disease.

Specific Aims

This study aims to determine how the metabolism of ovarian cancer spheroids differs from that of adherent ovarian cancer cells, and whether the addition of stromal cells such as endothelial cells, stromal vascular fraction of adipose tissue, and fibroblasts to spheroids causes any further metabolic shift or advantage. Further, the goal is to determine if changes in protein expression of metabolic markers or mitochondrial organization contribute to any metabolic changes observed in spheroids. By characterizing the metabolism of ovarian cancer spheroids and their metabolic interactions with other cell types, this project will identify novel targets for preventing metastasis and producing targeted treatments of this disease.

Aim 1 – Develop protocols for ovarian cancer spheroids to assess mitochondrial bioenergetics and to image mitochondrial network.

1A: Develop a protocol for measuring mitochondrial respiration in spheroids using a Seahorse XF24 Analyzer.

1B: Develop a method to stain spheroids with MitoTracker Red CMXROS dye and use confocal imaging to examine the mitochondrial network in homogeneous and heterogeneous spheroids.

Rationale: Spheroid formation has been shown to alter the properties of several cancer cell types. This allows the cancer cells, in spheroid form, to survive and metastasize better. An altered metabolism may be one of the contributing factors and understanding those changes would be advantageous for clinical purposes. The Seahorse Analyzer produces real-time, functional measurements that are valuable for examining metabolism. Furthermore, changes in metabolism seen in spheroids may be due to alterations in the mitochondrial network. Thus, imaging the mitochondria in homogeneous and heterogeneous spheroids may provide insight into differences seen in metabolism.

Aim 2 - Determine changes in metabolism of ovarian cancer cells.

2A: Determine changes in metabolism of ovarian cancer cells from adherent to 3D culture.

2B: Determine differences in metabolism of homogenous and heterogeneous ovarian cancer spheroids

Rationale: The aggressiveness and metastatic potential of MOSE ovarian cancer cells and TICs change both with progression of the disease and in 3D culture. This evidence necessitates an understanding of how metabolic changes may contribute to these observations.

Hypothesis: Spheroids will rely largely on glycolysis for fuel but will demonstrate functional mitochondria through oxygen consumption rate in bioenergetics analysis. Additionally, the spheroids with stromal cells will exhibit differing levels of oxygen consumption and glycolysis, likely relying less on glycolysis and more on utilizing substrates that the stromal cells prefer.

Aim 3 - Characterize protein expression profiles of metabolic biomarkers in ovarian cancer spheroids.

Rationale: In characterizing differences between the metabolism of adherent cancer cells, cancer cell-only spheroids, and cancer cell plus cargo cell combination spheroids, there is a need for elucidating potential underlying mechanisms for the observed differences. The underlying mechanisms, such as a change in protein expression, could ultimately serve as a clinical target. Targeting the underlying mechanisms of an observed change, rather than the change itself, could provide better clinical outcomes.

Hypothesis: Spheroids will exhibit protein expression profiles unique to each composition. Additionally, differences in metabolism between spheroid types will be [partially] explained by increased or decreased expression of certain key metabolic proteins.

III. MATERIALS AND METHODS

Cell Culture

MOSE cells were cultured in DMEM (Sigma) supplemented with 5% FBS (Atlanta Biologicals). In a previously described method, the cells were classified into the following phenotypes: early-benign (MOSE-E), intermediate (MOSE-I), and late-tumorigenic (MOSE-L).[12] For the experiments in this study, MOSE-L_{TICv} cells were used. To obtain MOSE-L_{TICv}s, MOSE-L cells ($1x10^6$ cells) were injected intraperitoneally (IP) into syngeneic C57BL/6 female mice. After 8 weeks, tumor cells were harvested from ascites and propagated in cell culture for 4 passages to eliminate all other cell types. These cells were subsequently transduced with firefly luciferase lentiviral particles (GeneCopeia) and transfected with pIRES-EGFP (ClonTech) to express the enhanced green fluorescent protein (EGFP).[54] Cells were cultured at 37°C in a

humidified incubator with 5% CO_2.

Three classes of other cells were used for the mitochondrial respiration assays, both in adherent and combination spheroid forms. These cells represent potential recruits from the peritoneal cavity or the SVF from adipose tissue with cancer-mediated differentiation of stem/progenitor cells into endothelial or fibroblasts. MILE SVEN 1 (MS1) murine endothelial cells obtained from ATCC and murine OP9 fibroblasts (ATCC® CRL-2749™) were cultured in DMEM supplemented with 5% FBS and 20% FBS, respectively, in a humidified incubator at a temperature of 37°C with 5% CO2. The cells comprising the stromal vascular fraction of white adipose tissue (SVF) cells were harvested from female C57BL/6N mice (see below) and frozen for storage in liquid nitrogen until time of use. At the time of use, SVF cells were thawed and cultured in DMEM supplemented with 5% FBS and allowed to grow to 80% confluence (without passaging).

Animals

Female C57BL/6N mice (Harlan Laboratories) were housed five per cage in a controlled environment for 6.5 months. The environment consisted of a 12 hour light/dark cycle at 21°C with unrestricted access to water and food. The diet was a high fat containing 60% kcal from fat (lard). At approximately 7 months of age when the average body weight of the mice reached 40g, mice were sacrificed by CO_2 asphyxiation. All animal procedures were conducted in accordance with the guidelines of the Virginia Tech Institutional Animal Care and Usage Committee (IACUC).

Tissue Digestion and Isolation of SVF

SVF cells were isolated from the visceral fat pads of white adipose tissue (WAT) of female C57BL/6N mice on a high fat (60% of kcal from fat) diet, according to standard

protocol.[56] In brief, WAT (mostly parametrial) was removed from the mice immediately after sacrifice and rinsed in Krebs-Ringer buffer (KRB), minced, and digested in collagenase solution (1 mg type IV collagenase, 10 mg BSA, and 2 mM CaCl2 in 1 ml PBS). The tissue was digested for 1 hour in a 37°C water bath and shaken every 5-10 minutes, then centrifuged at 300xg to separate the SVF from adipocytes. Oil and primary adipocytes were aspirated and the SVF pellet was resuspended in PBS with 1%BSA, then centrifuged again to ensure complete separation from adipocytes. The remaining cells were then plated in tissue-culture treated flasks in high glucose DMEM supplemented with 5% FBS and ciprofloxacin. After 24 hours, the medium was removed to eliminate dead cells. Attached cells were washed with PBS and plated in fresh medium (DMEM high glucose 5% FBS). Cells were used either directly or in the first passage after thawing.

Spheroid Growth

MOSE-L_{TICv} cells were seeded at 100,000 cells per well in 24-well ultralow adherence plates, spun for 3 min at 900rpm, and allowed to grow for 24 h at 37°C in a humidified incubator with 5% CO_2. At this time, all cells were incorporated in small spheroids. Spheroids were grown in DMEM supplemented with 5% FBS. For heterogeneous spheroids, cells were seeded 2:1 for MOSE-L_{TICv}:MS1 and MOSE-L_{TICv}:SVF. In MOSE-L_{TICv}:OP9 spheroids cells were seeded 4:1. These ratios were chosen to optimize growth of spheroids.

Mitochondrial Respiration

Mitochondrial respiration was determined using an XF24 extracellular flux analyzer (Seahorse Bioscience) essentially as described by Gerencser et al. for adherent cells with modifications for spheroids.[57]

Adherent

Cells were seeded into XF24 V7 cell culture microplates at a density of 35,000 cells per well for MOSE-L_{TICv} controls and 50,000 cells per well for MS1, SVF, and OP9 cells and incubated for 24 h in replicates of five. Then the medium was changed and the experiments were conducted in serum-free, bicarbonate-free medium after 1 h incubation. Cells were loaded into the XF24 and experiments consisted of 3-minute mixing, 2-minute wait, and 3-minute measurement cycles. Oxygen consumption rate (OCR) was measured under basal conditions in the presence of the mitochondrial inhibitors 0.5μmol/L oligomycin (Calbiochem) or 0.25μmol/L rotenone (Sigma), or in the presence of the mitochondrial uncoupler, 0.3μmol/L carbonylcyanide-p-trifluoromethoxyphenylhydrazone FCCP (Sigma) to assess maximal oxidative capacity. All experiments were performed at 37°C.

Western Blotting

Homogeneous and heterogeneous spheroids were grown as described above but in 6-well ultralow adherence plates at 3 million cells per well. Protein was extracted after transferring spheroids to 15 mL conicals for spins and washing with PBS to ensure removal of all media. Approximately 300 microliters of RIPA lysis buffer supplemented with Complete Mini Protease Inhibitor Cocktail (Roche) was added for cell lysis. Protein extraction beads (Diagenode's Bioruptor) were used for homogenization. Cells were also grown in adherent conditions in homogeneous and heterogeneous conditions and protein was extracted following the same method. Equal amounts of proteins were separated using 10% gels, transferred to PVDF membrane (Bio-Rad), and blocked with blocking buffer (Rockland). Blots were probed with primary antibodies against fatty acid binding protein 4 (FABP4), glutamine:fructose-6-phosphate amidotransferase (GFAT1), and pyruvate kinase (PKM2) followed by incubation with the

appropriate secondary antibodies. Gamma tubulin was loaded as a housekeeping protein. Proteins were visualized and quantitated using the Odyssey Infrared Imaging System (Licor).

Mitochondrial Staining

Spheroids were grown in 6-well ultralow adherent plates at 100,000 cells per well. Spheroids were then transferred to a 12-well plate and grown for 6 hours on cover slips. Next they were washed 2X with PBS before being incubated for 30 min in 50nM of MitoTracker Red CMXRos (Invitrogen) at 37°C in a humidified incubator with 5% CO_2. Next the spheroids were washed again and fixed with 3% paraformaldehyde for 30 min at room temperature. The paraformaldehyde was quenched by incubating the spheroids in 1.5 mg glycine/mL PBS for 10 min at room temperature. After a final wash with PBS, cover slips were transferred to glass slides and placed on a drop of antifade without DAPI (Thermo Fisher Scientific). Confocal microscopy was used to image the stained spheroids.

Statistics

All data are presented as mean ± SEM. When comparing multiple forms results were analyzed with a one-way ANOVA followed by Tukey's post ad hoc test. For two component comparisons data were analyzed using a student's two-tailed *t-test.* All results were analyzed by Prism (GraphPad). Results were considered significant at $p<0.05$

IV. RESULTS

Previous studies have demonstrated that in line with the Warburg effect, MOSE cells increase glycolysis as they progress and exhibit increased proliferation and tumorigenicity.[14] However, it was also shown that MOSE-L_{TICv} cells, which represent a variant population of cells that can cause recurrent disease after chemotherapy, exhibit a distinctly different metabolic

phenotype from their precursor population of MOSE-L cells. The MOSE-L_{TICv}s had a higher glycolytic reserve and ability to increase flux through the glycolytic pathway when oxidative phosphorylation was slowed or inhibited. They were also metabolically more flexible than their counterparts and were able to significantly increase oxygen consumption rate when their mitochondria were uncoupled, and overcome ATP synthase inhibition via oligomycin by increasing glycolysis.[19] However, it is unknown whether this metabolic phenotype remains when MOSE-L_{TICv}s aggregate into homogeneous or heterogeneous spheroids, with stromal cells incorporated into the latter. Since the tumor-initiating cell populations contribute to recapitulation of fatal disease in women, and spheroids have been shown to increase the survival and rate of metastatic success, this study assessed changes in the metabolism of MOSE-L_{TICv} cells from adherent to 3D culture and in homogeneous and heterogeneous spheroids with the goal of better understanding spheroid survival and identifying novel targets for ovarian cancer.

Development of mitochondrial bioenergetics analysis protocol for spheroids

To investigate the metabolism of ovarian cancer spheroids using real-time, functional measurements in a Seahorse XF24 extracellular flux analyzer a method had to be developed to effectively and accurately conduct analyses. Neither a protocol nor the specifically manufactured plates previously existed for conducting measurements on spheroids in an XF24 analyzer. The first trial method aimed to simply transfer spheroids to a standard, Seahorse-manufactured cell culture plate and allow them to adhere slightly. Slight adherence would mitigate movement during the experiment but would maintain the 3-dimensional structure. In Figure 8A a spheroid that has attached to a tissue-cultured plate for 12 hours is shown with an extracellular matrix outgrowth surrounding all edges. Initially, spheroids were grown in ultralow adherent 96-well

dishes to form uniform, multicellular spheroids. These spheroids were then transferred to a tissue-cultured plate using a pipette.

A **B**

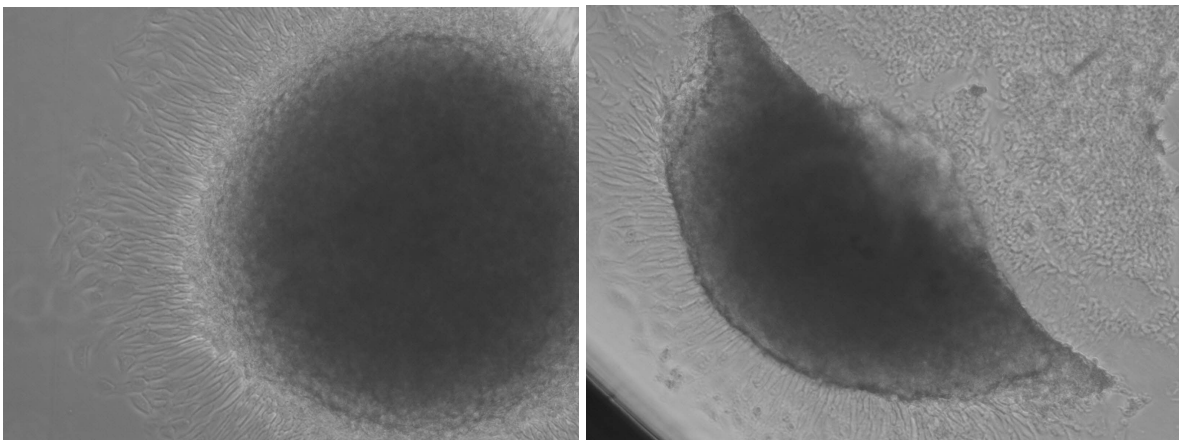

Figure 8. (A) A semi-attached spheroid in a tissue cultured plate. The spheroid was transferred from an ultralow adherence plate for growth to the standard Seahorse cell culture plate. Outgrowths onto the plate surround the spheroid on all edges. (B) A spheroid that has been damaged by the probe during a run. The spheroid is still attached to the plate as evidenced by the outgrowths.

The main issue that developed with using the standard Seahorse XF24 V7 cell culture microplate was that the dimensions of the well did not comfortably accommodate the size of a spheroid. During a run, probes are lowered into the well to deliver the inhibitors and take measurements of the extracellular flux. An adherent monolayer of cells remains in contact with the plastic bottom and does not interfere with this process, but a spheroid, even of small size (10,000 cells), could potentially be damaged by the probe (Figure 8B).

The next method of approach was to use an alternative plate that was already manufactured for an XF24 machine but would potentially better accommodate the spheroids; an XF24 islet capture microplate. This plate was originally developed to hold intact pancreatic islets and thus had slightly larger dimensions. As pictured in Figure 9, a dip in the bottom of each well produces a 3-dimensional space where the probe does not reach.

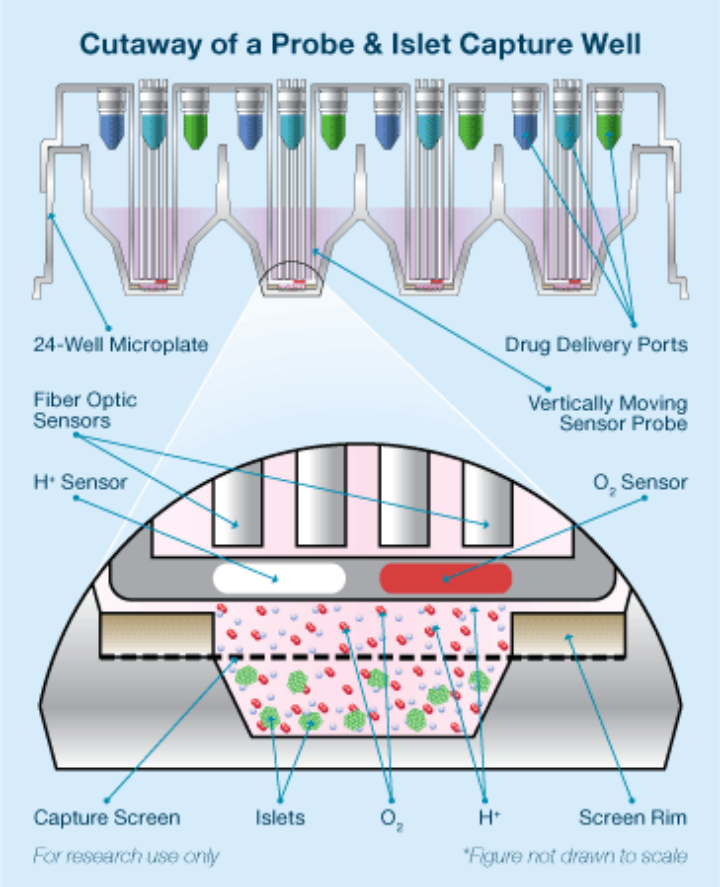

Figure 9. Visualization of islet capture microplate well and interaction with probe during a run. The sensor does not reach as close to the bottom of the well as it would in a cell culture plate with an adherent monolayer of cells, since pancreatic islets are a tissue, not a monolayer. Image from *Seahorse Bioscience*.

The islet plate did indeed prove to be a better 3-dimensional environment for the spheroids, but the next necessary step was to optimize the injections to elicit accurate measurements of uncoupled respiration and mitochondrial inhibition. Firstly, Seahorse Bioscience recommended increasing the number of loops for each measurement type in the protocol during a run. A standard format is shown in Figure 10, where 3 replicates are taken for each type of measurement (basal, inhibition with oligomycin, uncoupling with FCCP, and inhibition with rotenone and/or antimycin A). However, a total of 31 measurements was recommended for spheroids with 5 at basal, 12 after oligomycin, and 7 after FCCP and rotenone + antimycin A. This was to ensure that injection compounds had sufficient time to enter the spheroids and

interact. In a monolayer environment the cells immediately come in contact with the inhibitors but for spheroids diffusion through a larger, 3-dimensional structure has to occur.

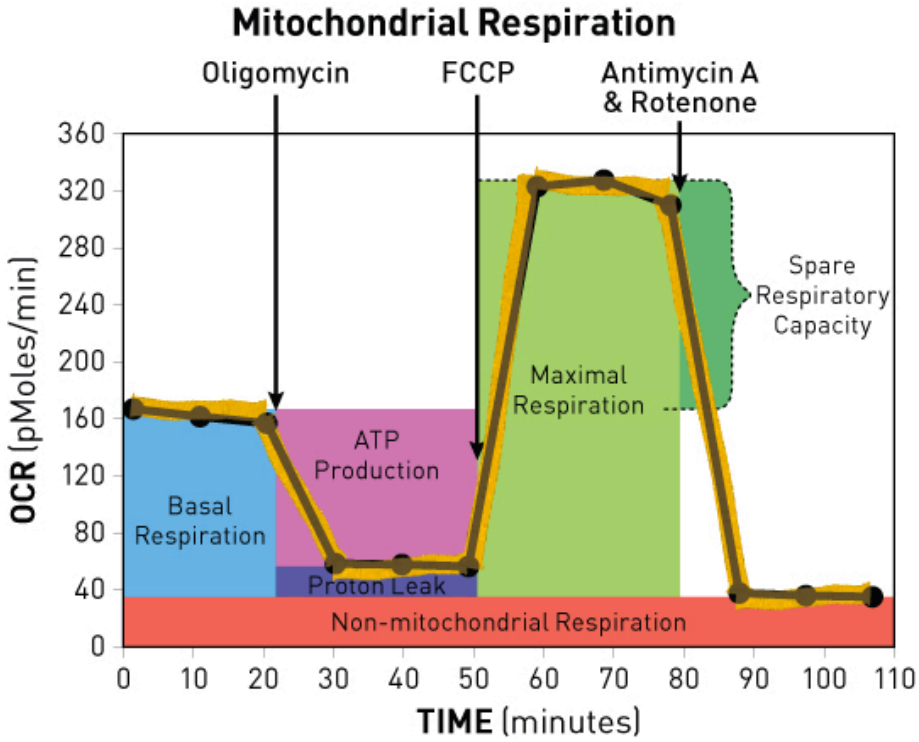

Figure 10. Depiction of a standard Seahorse protocol and the representative measurements taken over 2 h. Three measurements are taken during each condition. Image from *Seahorse Bioscience.*

In addition to an increased number of measurements, the optimal injection concentrations had to be identified for each injection type as well as optimal spheroid size/cell number. An initial run with varying spheroid sizes and number of spheroids per well immediately demonstrated that injection concentrations would have to be significantly altered as compared to the adherent culture concentrations, since none of the wells exhibited a significant response to the compounds (Figure 11). Wells were loaded with either 3 spheroids of 5,000 cells, 1 spheroid of 10,000 cells, 3 spheroids of 10,000 cells, 1 spheroid of 20,000 cells, or 1 spheroid of 50,000 cells, all in replicates of 4. This trial run aimed to investigate whether larger spheroids would create sufficient signal and whether clusters of smaller spheroids could respond equally well.

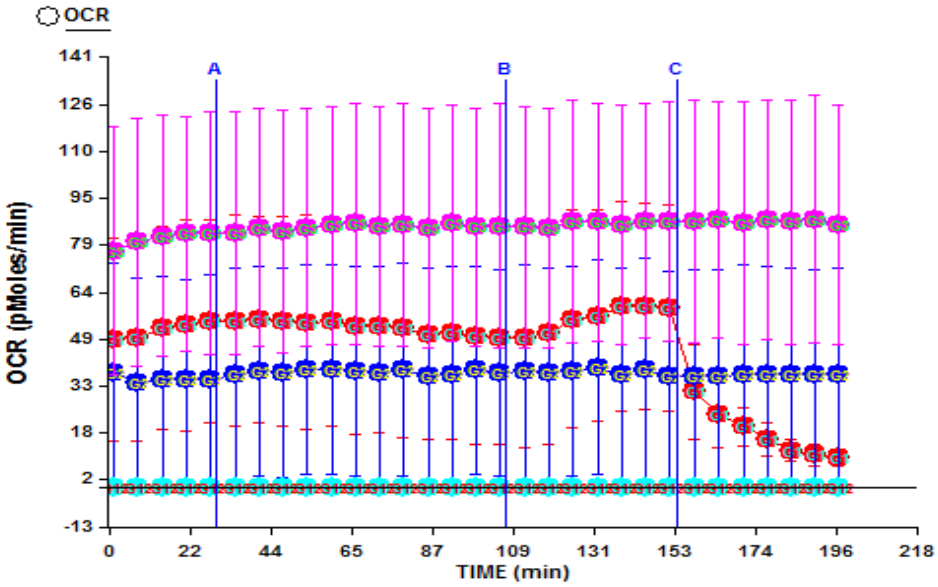

Figure 11. Trial experiment with spheroids of varying sizes and varying numbers of spheroids per well. In this tracing there is a large amount of standard error for each measurement, and the injections do not elicit the intended response from the cells.

To investigate optimal injection concentrations, spheroids of uniform size/cell number were loaded into a plate and varying injection concentrations for one injection type were loaded across the injection cartridge. That is, wells in replicates of at least 3 were loaded with constant concentrations of 2 injections and varying concentrations of 1 injection, so that the effect of concentration of one inhibitor could be isolated. In Figure 12 an example of a run conducted to optimize the concentration of oligomycin, the ATP synthase inhibitor, is shown. Concentrations of 1 μM and 2.5 μM were used in this case. Little difference was initially observed between the two concentrations, but in both cases very few wells on the plate responded and there was a high level of variability across the plate (Figure 12B).

A

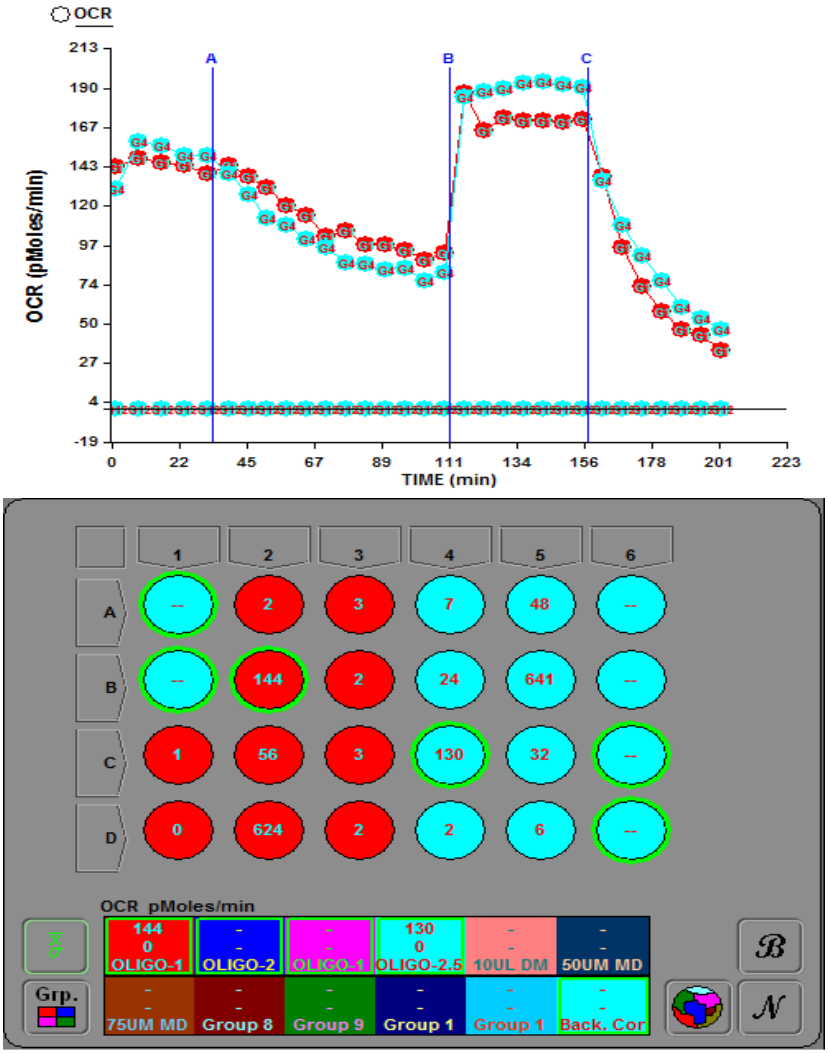
OCR
OCR (pMoles/min)
TIME (min)
A
B
C
213
190
167
143
120
97
74
50
27
4
-19
0
22
45
67
89
111
134
156
178
201
223
1
2
3
4
5
6
A
B
C
D
--
2
3
7
48
--
--
144
2
24
641
--
1
56
3
130
32
--
0
624
2
2
6
--
OCR pMoles/min
144
0
OLIGO-1
OLIGO-2
OLIGO-1
130
0
OLIGO-2.5
10UL DM
50UM MD
75UM MD
Group 8
Group 9
Group 1
Group 1
Back. Cor
Grp.

B

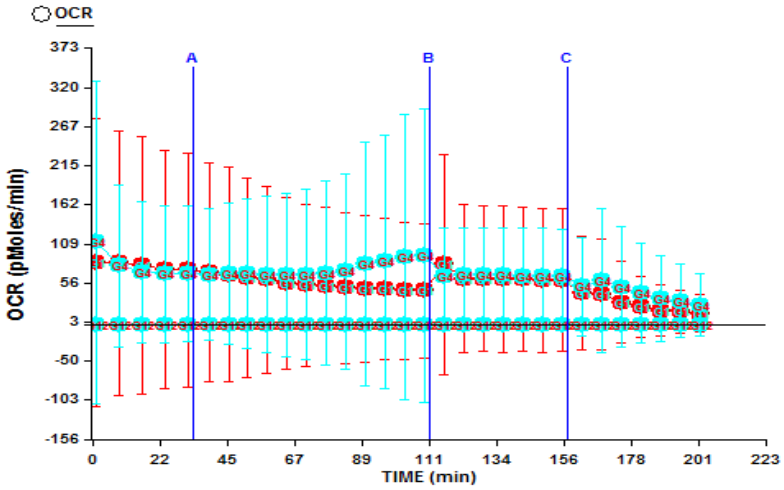
OCR
OCR (pMoles/min)
TIME (min)
A
B
C
373
320
267
215
162
109
56
3
-50
-103
-156
0
22
45
67
89
111
134
156
178
201
223

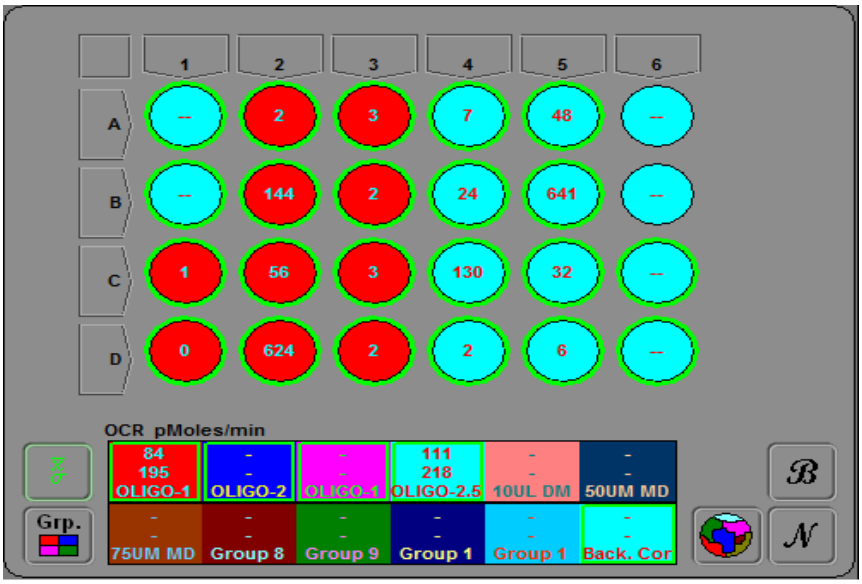

Figure 12. Tracings and their corresponding plate views from an experiment to optimize the concentration of oligomycin. (A) Response of wells that worked best with all 3 injections and the corresponding plate view showing how many wells selected are shown on the graph. (B) The same experiment but including all wells on the plate. With all wells included in the tracing, there is a high level of variability and poor response to injections.

Subsequent experiments such as those shown in Figure 12 produced more optimal concentrations for each injection type. However, a high level of variability across the plate still remained for each run and the signal response, even at basal levels, was poor. This indicated the need for larger spheroids (higher cell number) and perhaps a less stress-inducing form of transfer from the growth plate to the Seahorse plate.

At the start of optimization spheroids were being grown in a 96-well ultralow adherence plates that would produce one uniform spheroid in each well. However, these spheroids were limited in cell number as the viability of a large spheroid could not be sustained, and, thus, the spheroids would die quickly. More so, in order to transfer these spheroids, a 20 μL pipette tip was cut and used to draw the spheroid out of the well and be placed into the Seahorse plate; it was random where the spheroid would subsequently adhere to the Seahorse plate. This likely

contributed to the poor signal seen in many wells as the probe must be directly above the sample to get the best measurement.

To overcome these obstacles, we used a 24-well ultralow adherence plate to grow the spheroids and seeded them at 100,000 cells per well as opposed to the lower seeding number in 96-well dishes at 50,000 or below. The size of these spheroids are not uniform but instead are a cluster of many smaller, viable spheroids of varying, albeit comparable size. These are easier to transfer and easier to manipulate once placed in the Seahorse plate, allowing for better placement in the well. Indeed, this method elicited a more consistent response across the plate, and the injections had their intended effect (Figure 13). This suggested that a cell number of >50,000 cells is necessary to generate a consistent, reproducibly measurable response, and that large, uniform spheroids do not respond because the cells were not viable. Thus, moving forward this was the chosen approach. For the final protocol after all the spheroid size, injection concentration, and other optimizations were complete, the method, in brief, is as follows:

Spheroids are grown for 24 hours in a 24-well ultralow adherence dish and transferred to an islet capture plate using a transfer pipet. They are incubated in the islet plate overnight (12 h) to allow for a slight adherence to the plate. Then the medium is changed to standard Seahorse cell culture medium (DMEM, serum-free, bicarbonate-free) and the plate is incubated for 1 h in the Seahorse incubator. The plate is loaded into the XF analyzer and experiments consisted of 3-minute mixing, 1-minute wait, and 3-minute measurement cycles for the first injection (oligomycin), and 3-minute mixing, 0-minute wait, and 3-minute measurement cycles for the two subsequent inhibitors (FCCP and rotenone + antimycin A). OCR I s measured in the presence of the mitochondrial inhibitors 1.0 μmol/L oligomycin (Calbiochem) or 1.0 μmol/L rotenone + antimycin A (Sigma), or in the presence of the mitochondrial uncoupler, 3.0 μmol/L

carbonylcyanide-p- trifluoromethoxyphenylhydrazone FCCP (Sigma) to assess maximal oxidative capacity. This methodology provides a reliable and reproducible technique to investigate the mitochondrial bioenergetics of homogeneous and heterogeneous spheroids.

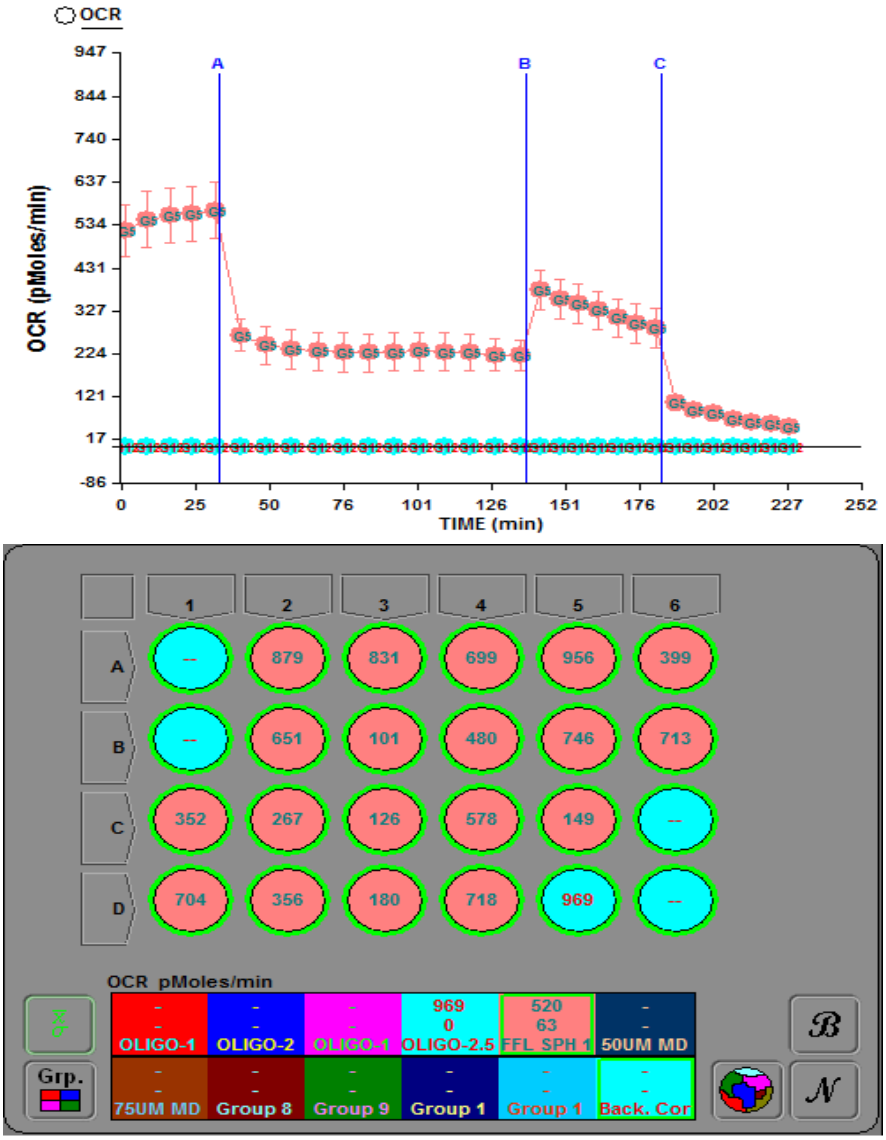

Figure 13. Tracing and corresponding plate view of optimized experiment. Very small standard error is seen for each measurement and the expected response to each injection is exhibited. On the plate, there is less variation among wells and higher consistency across the plate.

Development of mitochondrial staining method in spheroids

In order to visualize the mitochondria residing in ovarian cancer spheroids, we developed a staining method using MitoTracker Red CMXRos. This dye is red-fluorescent, accumulating in active mitochondria. Firstly, we established an optimized concentration and incubation time of the dye for staining in adherent MOSE-L_{TIC}s. Next, we optimized the method for fixing spheroids on a glass cover slip such that they could be imaged using confocal microscopy. Spheroids needed to retain 3-dimensional structure and therefore could not be placed between a slide and cover slip in mounting medium. This would have resulted in air bubble formation and damaged spheroids. Spheroids could not be imaged directly in their growth plate either, as plastic obstructs the light path and working distance of the microscope. Given these challenges, we attempted to grow spheroids and transfer them to a 25mm circular cover slip, placed in a 12-well cell culture dish. In this way, spheroids could adhere slightly allowing for washes, aspiration, etc. to be conducted without losing spheroids. More so, spheroids could then sit atop the slip and be stained, washed, fixed, and prepared for imaging without further transfers. A Zeiss LSM 880 confocal laser scanning microscope was used for imaging. This microscope can use inversion to image a 3-dimensional sample, therefore the cover slip was placed onto the microscope platform, directly above the objective lens.

These combined optimizations resulted in a successful method of imaging the mitochondria in ovarian cancer spheroids. The resulting method is as follows:

Spheroids are grown for 24 hours in an ultralow adherence plate. After growth, they are transferred to a 25mm circular cover slip in a 12-well cell culture dish. Spheroids are allowed to attach for 6 hours and then stained with 150 nM MitoTracker Red CMXRos for 15 min. Then they are washed, fixed with paraformaldehyde, and mounting medium containing antifade with

DAPI is added to each slip. The plate is covered and cover slips are removed using tweezers when ready for imaging.

Cellular metabolism in adherent cells

To assess the ability of adherent cells (representing cancer cells in their original location) and spheroids (representing exfoliated metastatic cell clusters) to adapt their metabolism to varying microenvironmental conditions, we used the Seahorse extracellular flux analyzer to measure OCR and glycolysis rate indirectly via extracellular acidification rate (ECAR). First, we examined all the cell types individually in their adherent form (Figure 14A). FCCP functions as a mitochondrial uncoupler by inducing proton leak through the inner mitochondrial membrane, which decreases proton motive force. To compensate, cells increase OCR, providing a measure of a cell's maximal respiration capacity. In Figure 14B, the FCCP-stimulated OCR for the MOSE-L_{TICv}s is shown compared to that of the stromal cells to be used in the heterogeneous spheroids. MS1 and SVF cells appear to have a slightly higher capacity than MOSE-L_{TICv}; however, this was not statistically significant. In Figure 14C the glycolytic capacity of each cell type is pictured, the result of the maximum ECAR reached after the injection of oligomycin. Oligomycin effectively shuts down oxidative phosphorylation by inhibiting ATP synthase, driving cells to use glycolysis to maximum capacity. OP9s are the only cells with a statistically significant different capacity from MOSE-L_{TICv}, and have the lowest capacity of all four.

A

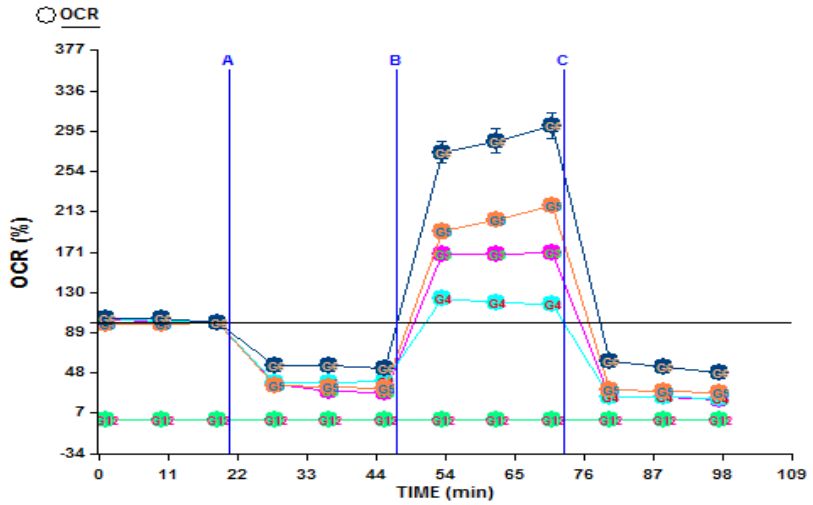

B

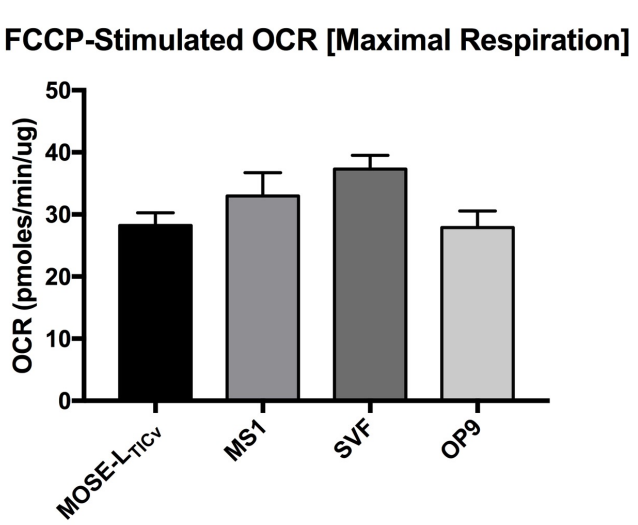

C

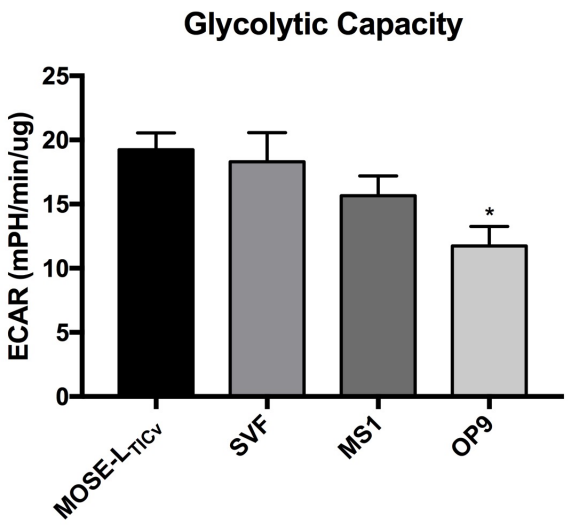

Figure 14. Assessment of extracellular flux in adherent cultures of MOSE-L_{TICv}, MS1, SVF, and OP9 cells. (A) Image of representative experiment measured over 2h. (B) maximal respiration levels in response to the mitochondrial uncoupler, FCCP. No significant differences present among the means. (C) Glycolytic capacity of adherent cells, represented by the maximum ECAR measure after the injection of oligomycin. Data are presented as mean +/- SEM.

Changes in cellular metabolism in response to 3D culture conditions

In contrast, there is a significant difference between the maximal respirations of MOSE-L_{TICv} in adherent form versus in spheroid form. Spare respiratory capacity is calculated using the

maximal respiration rate minus the basal respiration rate, indicating the capability of cells to respond to energetic demands and providing a measure of how closely cells are respiring to their theoretical maximum. As shown in Figure 15, the spare respiratory capacity of MOSE-L_{TICv} adherent cells is significantly larger than in spheroid form. A cell's ability to respond to varying demands can be an indicator of metabolic flexibility. The spheroids may either be functioning consistently at their maximum capacity or alternatively lose the ability of higher maximal capability due to their spheroid morphology.

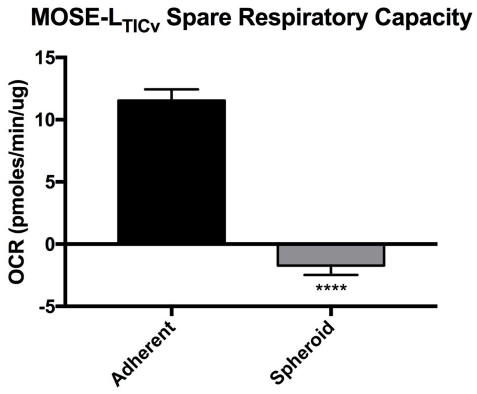

Figure 15. The spare respiratory capacity in adherent and spheroid forms of MOSE-L_{TICv}. Spare respiratory capacity is calculated by subtracting the basal respiration demand from the maximal respiration rate provided by mitochondrial uncoupling via FCCP. Data presented as mean +/- SEM, ****p<0.0001.

In fact, spheroids have a decreased metabolic capability across all metabolic measurements conducted in the extracellular flux assay compared to their adherent counterparts. They have a significantly lower basal respiration indicating a lower overall energetic demand under baseline conditions. (Figure 16A). The rate of ATP synthesis by the mitochondria is significantly lower in spheroids, perhaps in parallel to their overall lower energetic demand (Figure 16B). ECAR, a measurement of the rate of glycolysis, is also significantly lower compared to the adherent form (Figure 16C). Overall, these measurements indicate that MOSE-

$_{LTICv}$ spheroids exhibit less metabolic flexibility and overall lower levels of energetic activity than their adherent counterparts.

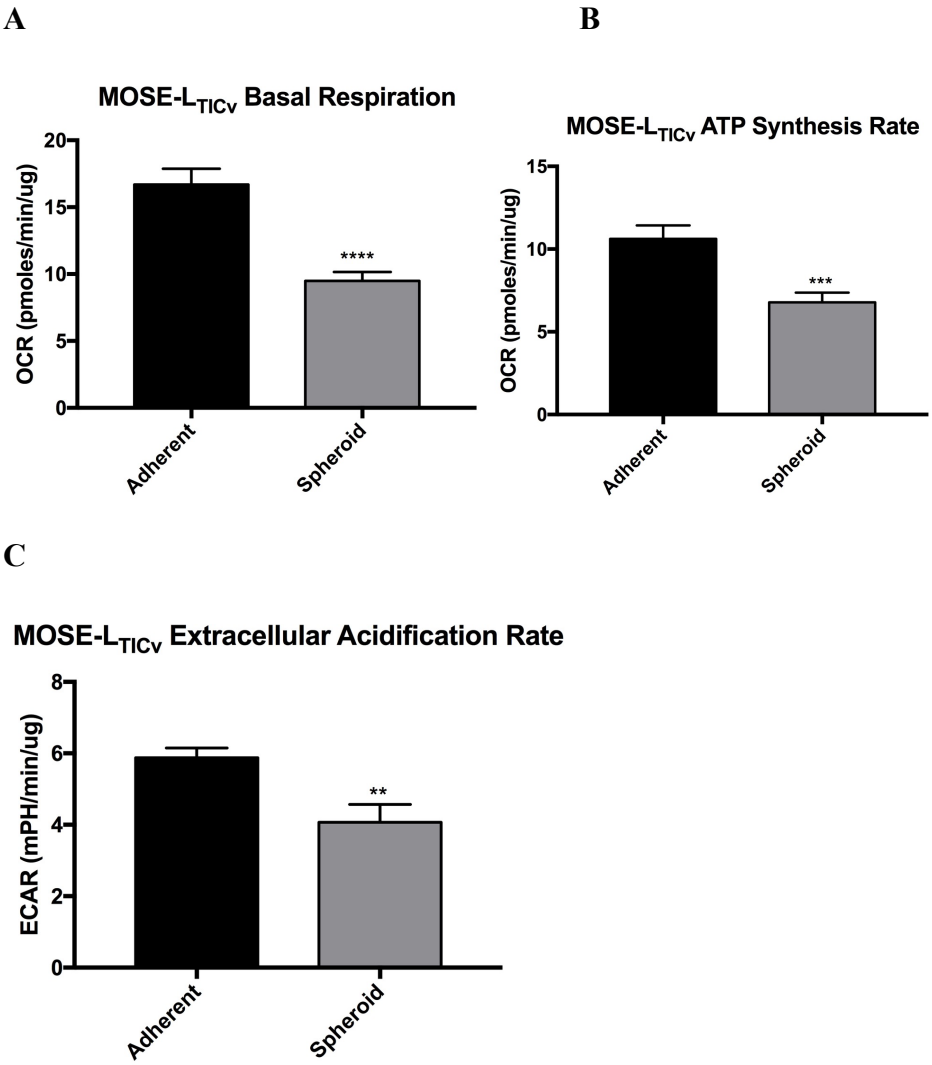

Figure 16. Measurements of basal respiration, ATP synthesis rate, and ECAR for MOSE-L_{TICv} in adherent and spheroid forms. (A) Basal respiration, representation of the basic energy demand. (B) ATP synthesis rate; the decrease in OCR upon injection of the ATP synthase inhibitor oligomycin represents the portion of basal respiration that is used to drive ATP production. (C) Oligomycin-stimulated ECAR; when ATP synthase is inhibited by oligomycin ATP production in the electron transport chain is blocked and cells must switch to glycolysis to produce energy. Data are presented as mean +/- SEM, ****p<0.0001, ***p<0.001, and **p<0.01.

Metabolic differences between heterogeneous and homogeneous spheroids

Next, the mitochondrial bioenergetics of homogeneous and heterogeneous spheroids were assessed to investigate whether the addition of stromal cells to a spheroid conferred any metabolic advantage. Previously it has been shown that the addition of stromal cells to ovarian cancer spheroids increases metastatic outgrowths, but little is known about the metabolic adaptations that occur.[55] Our results indicate that the addition of various stromal cell types does not provide any metabolic advantage or increased metabolic flexibility to spheroids. There were no significant differences among the means of the spare respiratory capacities of each spheroid type, an indicator of metabolic flexibility (Figure 17B). This is also evident in Figure 17A where the tracing of measurement points is shown, visualizing the representative experiment. Here, the maximum points for each group are clustered tightly, indicating that no cell type has a significantly larger capacity than any other. More so, ATP synthesis rate was significantly decreased in heterogeneous spheroids containing SVF and OP9 cells, and was almost equal to the rate in homogeneous spheroids when MS1 cells were included (Figure 17B, 17C).

In fact, glycolytic capacity was not increased in the heterogeneous spheroids, further characterizing them as metabolically inflexible (Figure 17D). Glycolysis in MOSE-L_{TICv}/SVF and MOSE-L_{TICv}/OP9 spheroids was significantly lower than in a homogenous spheroid. Interestingly, all heterogeneous spheroids exhibited a high level of non-mitochondrial respiration, which reached statistical significance in the MOSE-L_{TICv}/OP9 spheroids. This measure indicates the levels of oxygen consumption that persist due to a subset of cellular enzymes. Therefore, while these spheroids do not exhibit increased *mitochondrial* flexibility, it may be that other factors are contributing to oxygen consumption and/or energy production, and this could serve as a direction for future research.

A

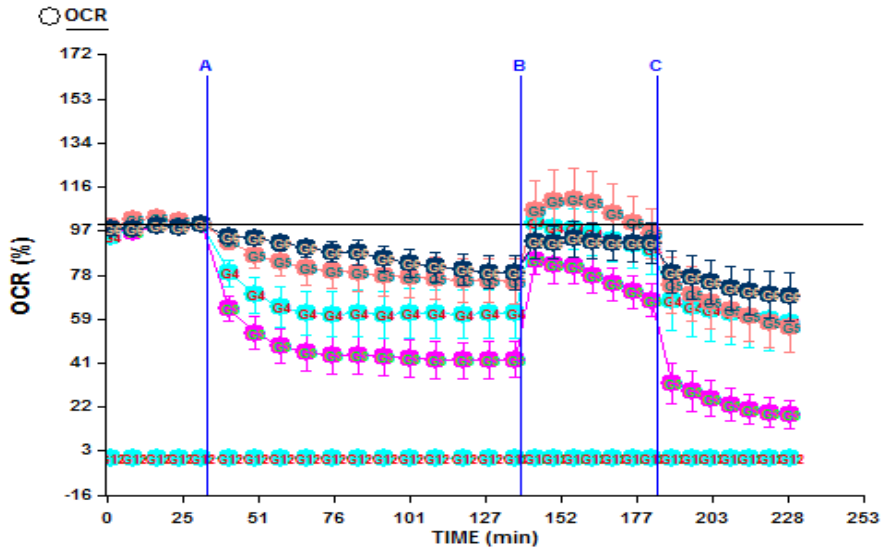
OCR
OCR (%)
TIME (min)
A
B
C

B

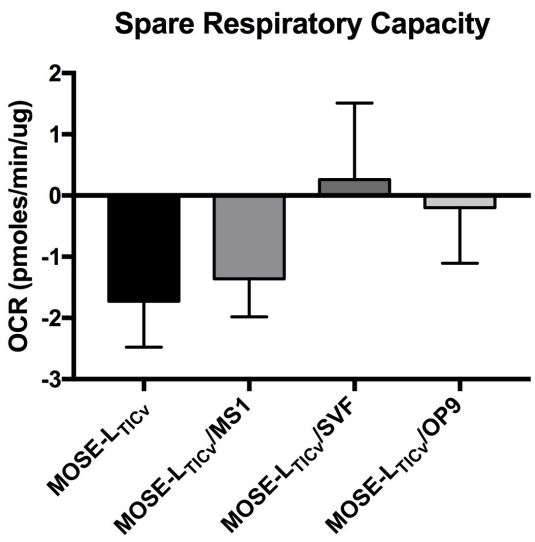
Spare Respiratory Capacity
OCR (pmoles/min/ug)
MOSE-L$_{TICv}$
MOSE-L$_{TICv}$/MS1
MOSE-L$_{TICv}$/SVF
MOSE-L$_{TICv}$/OP9

C

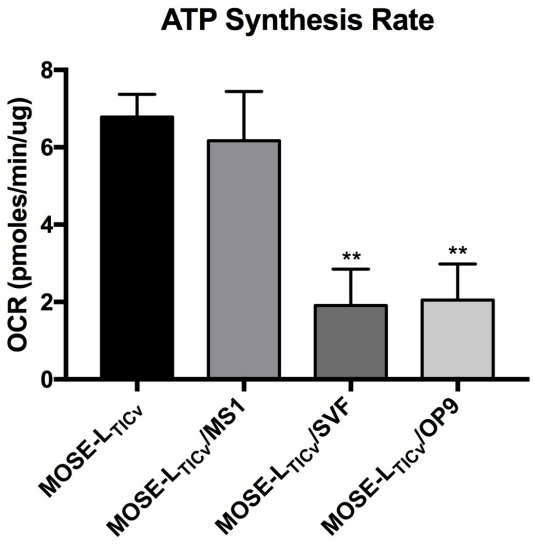
ATP Synthesis Rate
OCR (pmoles/min/ug)
**
**
MOSE-L$_{TICv}$
MOSE-L$_{TICv}$/MS1
MOSE-L$_{TICv}$/SVF
MOSE-L$_{TICv}$/OP9

D **E**

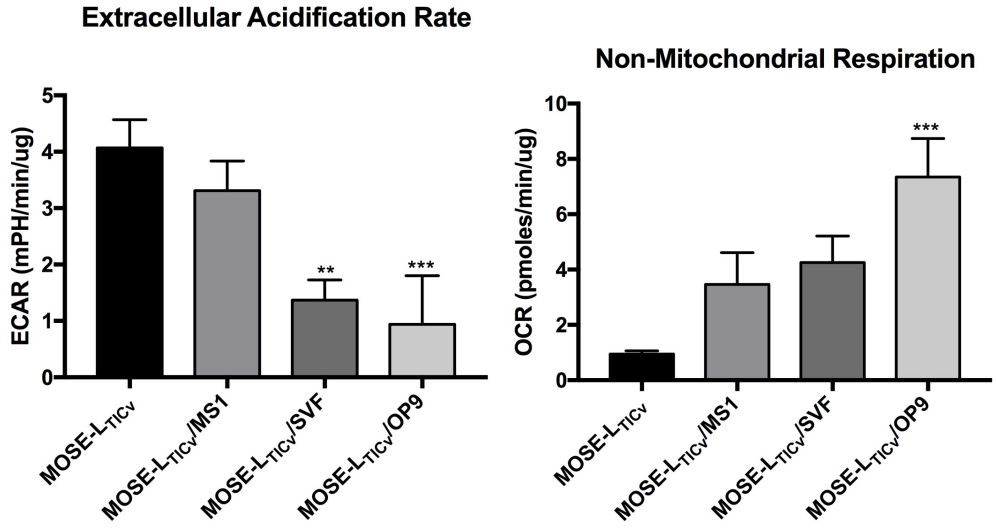

Figure 17. Assessment of metabolic parameters in homogeneous and heterogeneous ovarian cancer spheroids. (A) Image of representative experiment conducted over 4 h. (B) The spare respiratory capacity among each spheroid type. No significant difference was detected among any groups. (C) The ATP synthesis rate is decreased in heterogeneous spheroids with SVF and OP9 cells integrated. (D) ECAR, a measure of glycolysis, is decreased in spheroids with the addition of SVF and OP9 cells. (E) Non-mitochondrial respiration OCR in each spheroid type, with MOSE-L$_{TICv}$/OP9 spheroids exhibiting the highest rate. Data are presented as mean +/- SEM, ***p<0.001, and **p<0.01.

Mitochondrial organization in spheroids

As discussed previously, there is evidence indicating that the mitochondria found in cancer cells are functional despite their altered morphology; this was also observed in MOSE cells. In MOSE-E, the mitochondria are similar to those of regular epithelial cells, and as the disease progresses, the mitochondria are rounder and less organized. Even so, additional staining and flow cytometric analyses indicate that these mitochondria are functional. Additionally, we have observed that MOSE-L$_{TICv}$s are capable of intracellular transfer of mitochondria, a behavior that could be used to distribute healthy mitochondria throughout the cellular network. However, little is known about mitochondria structure or organization in spheroids and whether they are capable of intracellular transmission.

To gain a preliminary understanding of mitochondria in ovarian cancer spheroids, we stained homogeneous MOSE-$L_{TIC}v$ spheroids with mitotracker red and imaged them using confocal microscopy. Interestingly, the stain differs noticeably in the cells contained in the core versus those towards the adherent outgrowth edges. In the middle of the spheroid, the stain appears grainy, dispersed, and almost non-specific. However, we verified that it was unlikely that this was due to leakage because the cells at the outer edge were able to regain mitochondria and develop a clearer network (Figure 18).

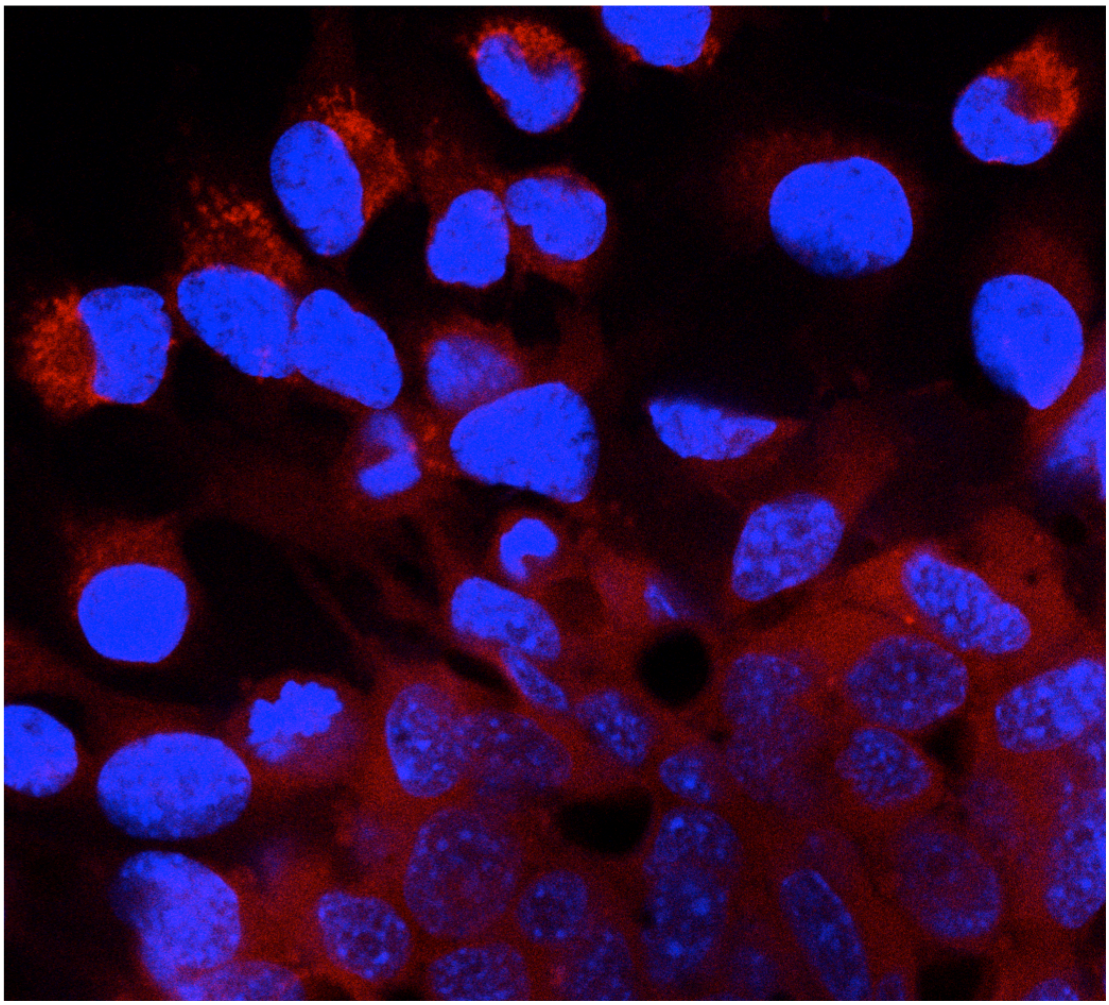

Figure 18. MOSE-L_{TICv} cells at the outer edge of a spheroid where they are attaching to the glass. DAPI (nuclear stain) is shown in blue and mitochondria in red (with mitotracker). A clear

network is not visible towards the center of the spheroid (bottom right of picture) where the mitochondria appear disintegrated. At the outer edge (towards top left) the mitochondria become clearer.

The spheroids also appeared to be capable of intracellular transfer of mitochondria as well. While evidence of intracellular nanotubular structures could be seen throughout the spheroid, it was more apparent towards the edges. It was also towards the edges where mitochondria could clearly be seen in these structures, likely being transferred from one cell to another (Figure 19). It is unclear which direction the mitochondria are moving; further experiments using time-lapse technology are needed to track their movement, and the impact of the transferred mitochondria for the cells' bioenergetics state.

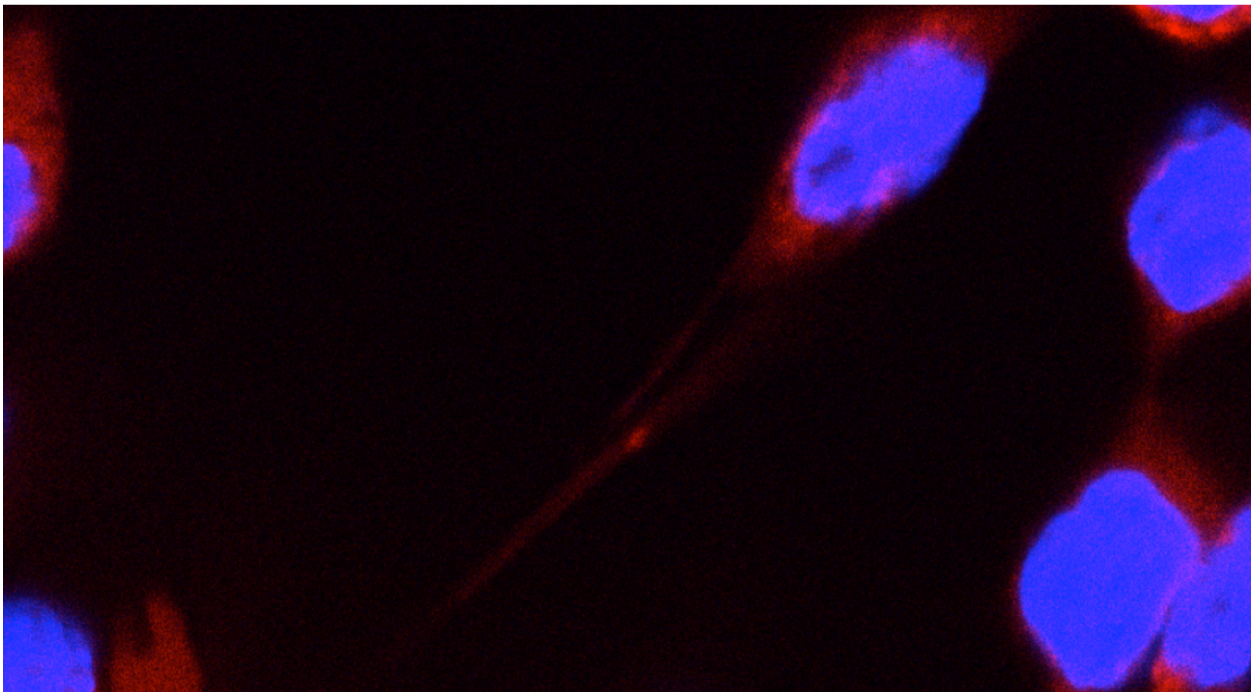

Figure 19. MOSE-L_{TICv} cells in spheroid formation, here shown at the outer edge of the structure where they begin to reattach. A mitochondrion can be seen in a tubular structure between two cells where there is a spot of increased red fluorescence.

Expression of proteins involved in cellular metabolism

In order to gain insight into underlying explanations for the metabolic differences observed among homogeneous adherent cells and spheroids as well as among homogeneous and

heterogeneous spheroids, preliminary analyses of metabolic protein expression levels were conducted. These data are procured from limited biological replicates, and may provide perspective on what might cause the significant differences among the metabolic profiles observed and could provide directions for future studies.

The first protein examined, glutamine:fructose-6-phosphate amidotransferase 1 (GFAT1), is a rate-limiting enzyme in the first step of the hexosamine biosynthesis pathway (HBP), which is a branch of the glucose metabolism pathway.[19] This pathway metabolizes 2-5% of cellular glucose. GFAT1 is one of two isoforms of GFAT, and is the major form that is expressed in various tissues and organs.[58] In previous studies of gastric cancer, low expression levels of GFAT1 were associated with unfavorable prognosis, as GFAT1 functioned as a suppressor of epithelial to mesenchymal transition (EMT).[40]

In the adherent cells and spheroids of homogeneous and heterogeneous types, adherent SVF and OP9 cells had the highest expression levels of GFAT1. All spheroids had relatively low expression levels, but MOSE-L_{TICv}/SVF spheroids did have higher expression levels than the other homogeneous and heterogeneous spheroids (Figure 20), which is likely due to the expression in the SVF rather than the result of heterogeneous spheroid formation.

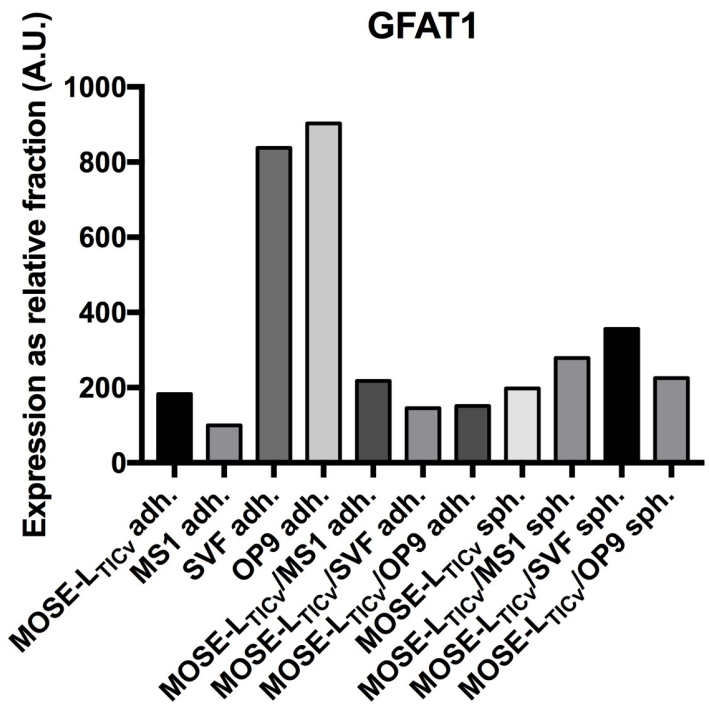

Figure 20. Expression levels of GFAT1 measured in adherent cells and spheroids of homogeneous and heterogeneous composition. Data are expressed as relative fractions in arbitrary units (A.U.) and normalized to the housekeeping protein γ-tubulin. Adherent SVF and OP9 cells exhibit the highest levels of expression among all groups. Heterogeneous SVF spheroids have the highest expression levels among all spheroid types.

Next, the protein expression level of pyruvate kinase (PKM2) was measured (Figure 21). PKM2 is considered a crucial enzyme in many cancers by contributing to the ability of cancer cells to achieve the nutrient demands of rapid proliferation. It is also considered a key player in the metabolic reprogramming that occurs in cancer cells as it is a limiting glycolytic enzyme that catalyzes the final step in glycolysis.[59] As discussed previously, cancer cells increase glycolysis in a phenomenon known as the Warburg effect, and therefore this pathway is crucial to their survival. Again, adherent SVF and OP9 cells had the highest expression levels. Spheroid formation increased PKM2 expression in MOSE-L_{TICv} but there was no difference to the heterogeneous spheroids.

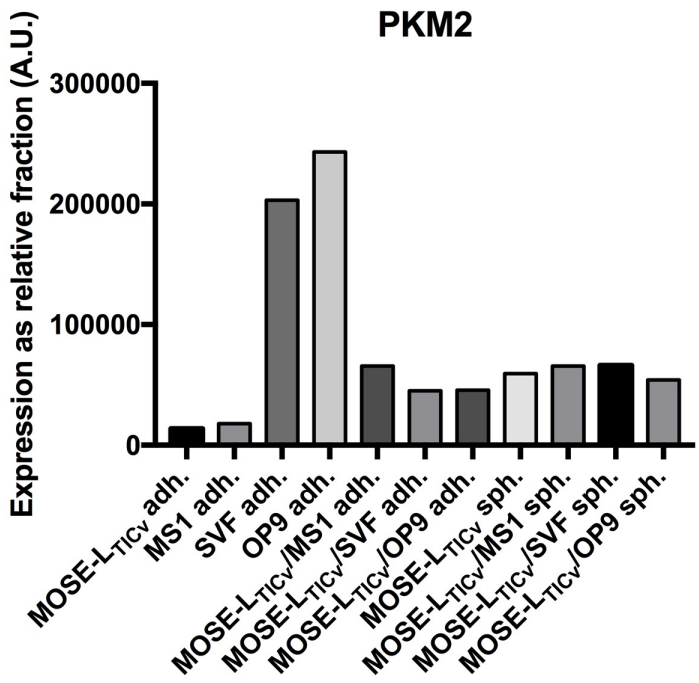

Figure 21. Expression levels of PKM2 measure in adherent cells and spheroids of homogeneous and heterogeneous subtypes. Data are expressed as relative fractions in arbitrary units (A.U.) and normalized to the housekeeping protein γ-tubulin. Adherent SVF and OP9 cells have the highest expression levels of all groups. All spheroid samples exhibit higher expression levels than adherent MOSE-L_{TICv}.

The final protein investigated in these cell populations was fatty acid binding protein 4 (FABP4). Previous studies have been conducted on FABP4 and cancer due to its key role in the ability of cancer cells to interact with adipocytes. FABP4 is highly expressed by adipocytes, macrophages, and dendritic cells.[60] In an earlier study, MOSE-L_{TICv} had significantly increased mRNA levels of FABP4 compared to MOSE-E and MOSE-L cells. However, our results as shown in Figure 22 show only FABP4 expression in adherent OP9 cells and MOSE-L_{TICv}/OP9 spheroids. The reason for this observation is unclear and so, further experiments investigating this protein in our cell line and in fibroblasts would be helpful.

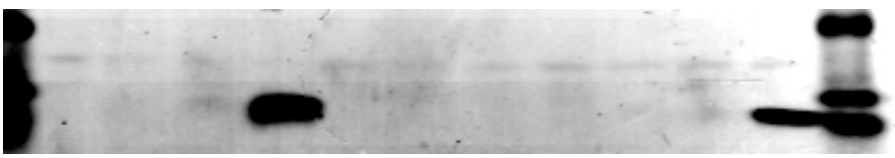

Figure 22. Western blotting of FABP4 resulting in high intensity bands in lanes 5 and 12, with adherent OP9 and heterogeneous OP9 spheroids respectively. FABP4 molecular weight is projected at 15 kDa. Other lanes show little to no signal.

Antibodies for acetyl coA carboxylase (ACC), fatty acid synthase (FASN), ELOVL fatty acid elongase 5 (ELOVL5), hexokinase 2 (HK2), pyruvate dehydrogenase kinase 1 (PDK1), and L-glutamine amidohydrolase (LGA) were also tested but did not procure sufficient signal in our cell lines. Ideally, working antibodies will be identified for these and other proteins to identify changes in expression levels related to the breakdown, synthesis, and transport of fatty acids, lipids, glucose, and glutamine in our cell lines.

V. CONCLUSION AND FUTURE DIRECTIONS

As ovarian cancer remains to be the leading cause of gynecological cancer death in women with a 50-70% relapse of the disease within 18 months following standard treatments, it is clear that better treatments are needed.[61] One potential target that could be responsible for the high relapse rate observed is the cell population that remains in the peritoneal cavity after surgery, aggregated and enriched in tumor-initiating cell populations that are capable of recapitulating the original tumor. In previous studies, these cells were characterized as more glycolytic than benign or late-stage cells and having increased metabolic flexibility.[19]

In the present study we provide an initial characterization of aggregates of MOSE-L_{TICv} cells. We demonstrate that the homogeneous cancer cell spheroids have a lower basal energetic demand than the adherent MOSE-L_{TICv} cells, and, accordingly, have a lower spare respiratory capacity and ATP synthesis rate. Spare respiratory capacity serves as an indicator of metabolic flexibility. The spheroids may consistently function at their maximal threshold, which would explain the lack of reserve capacity. The spheroids also demonstrated a lower basal energetic demand than adherent cells, so it is possible that this demand changes their phenotype to a less

flexible metabolism because of the lack of demand. We have previously shown that the cancer spheroids recruited stromal cells into the aggregates and that this confers a survival advantage and leads to the development of a highly metastatic phenotype. Our hypothesis was that this heterogeneous aggregation may allow the cancer cells to adapt metabolically. However, our data indicate that stromal cells do not confer any increases in spare respiratory capacity, ATP synthesis rate, or ECAR. It is possible that stromal cells confer other advantages in functional categories such as structure, invasiveness, angiogenesis, or others. However, the downregulation of energy expenditure may actually be an advantage in spheroids, with lower basal energy demands reflecting the ability to maintain survival rather than to support rapid growth. Other studies conducted in our lab demonstrated that spheroids in medium (non-adherent conditions) grow significantly slower than adherent MOSE-L_{TICv}. Future studies investigating how proliferation changes when spheroids adhere and invade tissues (the next step towards a successfully metastatic outgrowth) in conjunction with extracellular flux analyses might reveal that when spheroids are growing rapidly outwards they also experience changes in metabolism.

More so, examining the outgrowth rate and proliferation rate of homogeneous spheroids versus heterogeneous spheroids would be helpful to see if in invasive conditions, stromal cells do contribute to metabolic adaptation. It is possible that spheroid formation in the ascites activates signals to inhibit proliferation, and it is advantageous to suppress proliferation/rapid growth until attachment to the omentum, or mesenteric lining of the peritoneal cavity. . It is possible that cancer cells recruit stromal cells in the ascites, form a spheroid, and remain at that size with reduced proliferation but still gain the ability to develop metastatic outgrowths and survive longer with their diverse population of cells via changes in the expression of genes in functional categories other than metabolism. An increase in size may be achieved by recruiting cells rather

than proliferation. It is also important to consider that while this study provided preliminary insights into heterogeneity, under physiological conditions in the peritoneal cavity it is more likely that a microenvironment will consist of multiple cell types, not just two per spheroid as we investigated. In that case it is possible that interplay among the stromal cells is a key component in their ability to support the cancer cells.

In that line of thought, future investigations into spheroid heterogeneity should be conducted to identify ratios of cancer cells to stromal cells that may confer an advantage. In this study, heterogeneous spheroids were at 2:1 and 4:1 ratios, whereas in tumors it has been shown that there are a wide spectrum of cancer cell to stromal cell variations. It may be possible that spheroids with higher fractions of stromal cells than cancer cells are actually more metabolically flexible, or even exhibit distinct metabolic profiles from the ones examined here. It is also possible that an incubation period longer than 24 h would produce distinct metabolic differences in spheroids. As a spheroid evolves, perhaps the initial stages involve only organization and stability, and therefore require a lower energetic demand to sustain those. In subsequent stages the spheroids might increase growth and experience changes in metabolism to compensate. A pattern such as this would parallel the changes seen in MOSE cells from early to late stages as demonstrated in previous research. OCR, maximal respiration, and ATP synthesis rate decrease in a stepwise manner from MOSE-E, MOSE-I, to MOSE-L during progression.[14] It may be that cells in spheroids experience a progression of their own, from metabolically flexible MOSE-L_{TICv} to a downregulated phenotype initially with spheroid formation to a different, more active phenotype further into spheroid progression.

The distinct differences observed in the mitochondria of spheroids compared to those in adherent cells indicates the need for further imaging analyses of these organelles. The cells at the

outward-growing edge of a spheroid appear to regain mitochondria, where as core cells have a disorganized, perhaps even disintegrated network. It is unclear what is causing the changes in mitochondria throughout the spheroid, but it would be helpful to understand what causes the distinct change. It could be that disruptions in fission and fusion processes occur, resulting in highly disorganized mitochondria. Other studies have investigated fragmentation of mitochondria, such as in the case of uncoupling or inhibited respiration.[62] In these cases, researchers have reported the appearance of single mitochondria or "doughnut-like shapes".[41,63-65] It is possible that we are observing a similar effect in the spheroids. The spheroids demonstrated no spare respiratory capacity, which could mean that they are uncoupled and therefore are functioning at their maximum capacity (which may be low due to damaged membranes). Furthermore, they may have downregulated respiration, comparable to an inhibition effect, to parallel their slowed rate of proliferation. In that case, the mitochondrial morphology could be affected and mimic the small solitary mitochondria observed under chemical inhibition of respiration. It is also interesting that the mitochondria in the adherent outer edges of spheroids appear better organized, suggesting that they are still functional. Additionally, we observed intercellular transfer of mitochondria, so cells that have high-functioning mitochondria may send them to the core where they are needed.

Another interesting consideration in light of these results is the use of 5-aminoimidazole-4-carboxamide 1-ß-D ribo- furanoside (AICAR) in the treatment of cancer. AICAR is a monophosphate kinase (AMPK) agonist, and while usually used for treatment of diabetes, has been thought to show promise in the treatment of cancer. Previously, MOSE-L_{TICv} cells exhibited significantly more resistance to AICAR than MOSE-E and MOSE-L cells. This drug is aimed at modulating glucose utilization but as demonstrated here, the spheroids have a significantly lower

ECAR than the adherent cells. That being the case, it is possible that spheroids are able to remain dormant in the body even with the treatment of AICAR due to a) the inherent resistance of MOSE-L_{TICv} cells to AICAR and b) their low rate of glycolysis and low metabolic demand overall.

Another possible direction for future research would be to investigate spheroids comprised of MOSE-E cells and stromal cells. It has previously been observed that MOSE-E cells do not survive in ultralow adherent conditions over time but with the addition of stromal cells survival is increased (unpublished data). It is possible that metabolic changes occur earlier on and confer advantages to the early stage cells, contributing to progression of the disease and survival of those spheroids. If these changes were identified, they could serve as novel therapeutic targets in early stage disease, which is currently needed. It would also be beneficial to further investigate protein expression profiles, as the data presented here are strictly exploratory and unfortunately do not provide clear insight into the differences in bioenergetics observed.

The differences in protein expression levels reported here indicate that adherent SVF and OP9 cells have increased expression of PKM2 and GFAT1. In contrast, the glycolytic capacity reported indicates that SVF have a comparable glycolytic capacity to MOSE-L_{TICv}, and OP9 have a significantly lower glycolytic capacity than both. These results provide conflicting characterizations of glycolysis and its' role in these cells. MOSE-L_{TICv} did not have high expression of PKM2, suggesting that other enzymes are responsible for the glycolytic capacity measured in the extracellular flux analyses. Spheroids have increased PKM2 and GFAT1 compared to adherent MOSE-L_{TICv}, in contrast to the decreased rates of glycolysis and energy demand measured. Likely the increased expression in heterogeneous spheroids is a result of the

high expression in SVF and not due to spheroid formation. The increased levels of GFAT1 in spheroids reported here conflict with previous evidence associating low levels of GFAT1 with poor prognosis in gastric cancer.[40] One would expect that the association of spheroids with aggressive forms of ovarian cancer (and thus an unfavorable prognosis) would result in low levels of GFAT1, which is also an indicator of poor prognosis. Collectively, this evidence suggests that other proteins are key players in the metabolic differences observed in adherent cells, heterogeneous, and homogeneous spheroids.

While still very preliminary, our results indicate that ovarian cancer spheroids exhibit different metabolic profiles than their adherent counterparts, and that heterogeneous spheroids do not improve the metabolic flexibility of spheroids as expected. Thus, adaptations of the metabolism in cell aggregates may confer a survival signal that contributes to an enhanced metastatic outgrowth. This necessitates further examination of the molecular events that are activated by the interaction of stromal and cancer cells to improve the survival of spheroids and increase their metastatic potential; candidates are genes increasing survival, adhesion, motility, resistance to hypoxia and others. Furthermore, the unique demands of spheroids, both heterogeneous and homogeneous, require the development of drugs that specifically target these signaling events or overcome the ability of spheroids to survive on a low energetic baseline with little to no metabolic flexibility.

VII. References

1 Jemal, A. *et al.* Cancer statistics, 2008. *CA Cancer J Clin* **58**, 71-96, doi:10.3322/CA.2007.0010 (2008).

2 Liu, C. M. Cancer of the ovary. *N Engl J Med* **352**, 1268-1269; author reply 1268-1269 (2005).

3 Hogberg, T., Glimelius, B., Nygren, P. & Care, S. B.-g. S. C. o. T. A. i. H. A systematic overview of chemotherapy effects in ovarian cancer. *Acta Oncol* **40**, 340-360 (2001).

4 Kuk, C. *et al.* Mining the ovarian cancer ascites proteome for potential ovarian cancer biomarkers. *Mol Cell Proteomics* **8**, 661-669, doi:10.1074/mcp.M800313-MCP200 (2009).

5 Shield, K., Ackland, M. L., Ahmed, N. & Rice, G. E. Multicellular spheroids in ovarian cancer metastases: Biology and pathology. *Gynecologic oncology* **113**, 143-148, doi:10.1016/j.ygyno.2008.11.032 (2009).

6 Warburg, O. On the origin of cancer cells. *Science* **123**, 309-314 (1956).

7 Warburg, O., Wind, F. & Negelein, E. The Metabolism of Tumors in the Body. *J Gen Physiol* **8**, 519-530 (1927).

8 Zu, X. L. & Guppy, M. Cancer metabolism: facts, fantasy, and fiction. *Biochemical and biophysical research communications* **313**, 459-465 (2004).

9 Weinhouse, S. On respiratory impairment in cancer cells. *Science* **124**, 267-269 (1956).

10 Rossignol, R. *et al.* Energy substrate modulates mitochondrial structure and oxidative capacity in cancer cells. *Cancer research* **64**, 985-993 (2004).

11 Fantin, V. R., St-Pierre, J. & Leder, P. Attenuation of LDH-A expression uncovers a link between glycolysis, mitochondrial physiology, and tumor maintenance. *Cancer Cell* **9**, 425-434, doi:10.1016/j.ccr.2006.04.023 (2006).

12 Roberts, P. C. *et al.* Sequential molecular and cellular events during neoplastic progression: a mouse syngeneic ovarian cancer model. *Neoplasia* **7**, 944-956 (2005).

13 Creekmore, A. L. *et al.* Changes in gene expression and cellular architecture in an ovarian cancer progression model. *PloS one* **6**, e17676, doi:10.1371/journal.pone.0017676 (2011).

14 Anderson, A. S. *et al.* Metabolic changes during ovarian cancer progression as targets for sphingosine treatment. *Experimental cell research* **319**, 1431-1442, doi:10.1016/j.yexcr.2013.02.017 (2013).

15 Cohen, C. A., Shea, A. A., Heffron, C. L., Schmelz, E. M. & Roberts, P. C. Intra-abdominal fat depots represent distinct immunomodulatory microenvironments: a murine model. *PloS one* **8**, e66477, doi:10.1371/journal.pone.0066477 (2013).

16 Alvero, A. B. *et al.* Molecular phenotyping of human ovarian cancer stem cells unravels the mechanisms for repair and chemoresistance. *Cell cycle* **8**, 158-166, doi:10.4161/cc.8.1.7533 (2009).

17 Wani, A. A., Sharma, N., Shouche, Y. S. & Bapat, S. A. Nuclear-mitochondrial genomic profiling reveals a pattern of evolution in epithelial ovarian tumor stem cells. *Oncogene* **25**, 6336-6344, doi:10.1038/sj.onc.1209649 (2006).

18 Abubaker, K. *et al.* Short-term single treatment of chemotherapy results in the enrichment of ovarian cancer stem cell-like cells leading to an increased tumor burden. *Molecular cancer* **12**, 24, doi:10.1186/1476-4598-12-24 (2013).

19 Anderson, A. S., Roberts, P. C., Frisard, M. I., Hulver, M. W. & Schmelz, E. M. Ovarian tumor-initiating cells display a flexible metabolism. *Experimental cell research* **328**, 44-57, doi:10.1016/j.yexcr.2014.08.028 (2014).

20 Lengyel, E. Ovarian cancer development and metastasis. *Am J Pathol* **177**, 1053-1064, doi:10.2353/ajpath.2010.100105 (2010).

21 Zhang, Y. *et al.* Stromal Cells Derived from Visceral and Obese Adipose Tissue Promote Growth of Ovarian Cancers. *PloS one* **10**, e0136361, doi:10.1371/journal.pone.0136361 (2015).

22 Zhang, Y. *et al.* Stromal progenitor cells from endogenous adipose tissue contribute to pericytes and adipocytes that populate the tumor microenvironment. *Cancer research* **72**, 5198-5208, doi:10.1158/0008-5472.CAN-12-0294 (2012).
23 Chowanadisai, W. *et al.* Cisplatin Resistant Spheroids Model Clinically Relevant Survival Mechanisms in Ovarian Tumors. *PloS one* **11**, e0151089, doi:10.1371/journal.pone.0151089 (2016).
24 Barbolina, M. V. *et al.* Microenvironmental regulation of ovarian cancer metastasis. *Cancer Treat Res* **149**, 319-334, doi:10.1007/978-0-387-98094-2_15 (2009).
25 Naora, H. & Montell, D. J. Ovarian cancer metastasis: integrating insights from disparate model organisms. *Nat Rev Cancer* **5**, 355-366, doi:10.1038/nrc1611 (2005).
26 Allen, H. J., Porter, C., Gamarra, M., Piver, M. S. & Johnson, E. A. Isolation and morphologic characterization of human ovarian carcinoma cell clusters present in effusions. *Exp Cell Biol* **55**, 194-208 (1987).
27 Burleson, K. M., Boente, M. P., Pambuccian, S. E. & Skubitz, A. P. Disaggregation and invasion of ovarian carcinoma ascites spheroids. *J Transl Med* **4**, 6, doi:10.1186/1479-5876-4-6 (2006).
28 Zietarska, M. *et al.* Molecular description of a 3D in vitro model for the study of epithelial ovarian cancer (EOC). *Mol Carcinog* **46**, 872-885, doi:10.1002/mc.20315 (2007).
29 Ahmed, N., Thompson, E. W. & Quinn, M. A. Epithelial-mesenchymal interconversions in normal ovarian surface epithelium and ovarian carcinomas: an exception to the norm. *J Cell Physiol* **213**, 581-588, doi:10.1002/jcp.21240 (2007).
30 Lin, H. & Changchien, C. C. Management of relapsed/refractory epithelial ovarian cancer: current standards and novel approaches. *Taiwan J Obstet Gynecol* **46**, 379-388, doi:10.1016/S1028-4559(08)60007-8 (2007).
31 Piccart, M. J., Lamb, H. & Vermorken, J. B. Current and future potential roles of the platinum drugs in the treatment of ovarian cancer. *Ann Oncol* **12**, 1195-1203 (2001).
32 Moreno-Sanchez, R., Rodriguez-Enriquez, S., Saavedra, E., Marin-Hernandez, A. & Gallardo-Perez, J. C. The bioenergetics of cancer: is glycolysis the main ATP supplier in all tumor cells? *Biofactors* **35**, 209-225, doi:10.1002/biof.31 (2009).
33 Kallinowski, F. *et al.* Blood flow, metabolism, cellular microenvironment, and growth rate of human tumor xenografts. *Cancer research* **49**, 3759-3764 (1989).
34 Lim, H. Y., Ho, Q. S., Low, J., Choolani, M. & Wong, K. P. Respiratory competent mitochondria in human ovarian and peritoneal cancer. *Mitochondrion* **11**, 437-443, doi:10.1016/j.mito.2010.12.015 (2011).
35 Finkel, T. Signal transduction by mitochondrial oxidants. *The Journal of biological chemistry* **287**, 4434-4440, doi:10.1074/jbc.R111.271999 (2012).
36 Chan, D. W. *et al.* Loss of MKP3 mediated by oxidative stress enhances tumorigenicity and chemoresistance of ovarian cancer cells. *Carcinogenesis* **29**, 1742-1750, doi:10.1093/carcin/bgn167 (2008).
37 Andrews, P. A. & Albright, K. D. Mitochondrial defects in cis-diamminedichloroplatinum(II)-resistant human ovarian carcinoma cells. *Cancer research* **52**, 1895-1901 (1992).
38 John, G. B. *et al.* The mitochondrial inner membrane protein mitofilin controls cristae morphology. *Mol Biol Cell* **16**, 1543-1554, doi:10.1091/mbc.E04-08-0697 (2005).
39 Perry, S. W., Norman, J. P., Barbieri, J., Brown, E. B. & Gelbard, H. A. Mitochondrial membrane potential probes and the proton gradient: a practical usage guide. *Biotechniques* **50**, 98-115, doi:10.2144/000113610 (2011).
40 Duan, F. *et al.* Loss of GFAT1 promotes epithelial-to-mesenchymal transition and predicts unfavorable prognosis in gastric cancer. *Oncotarget* **7**, 38427-38439, doi:10.18632/oncotarget.9538 (2016).
41 Rustom, A., Saffrich, R., Markovic, I., Walther, P. & Gerdes, H. H. Nanotubular highways for intercellular organelle transport. *Science* **303**, 1007-1010, doi:10.1126/science.1093133 (2004).

42 Dier, U., Shin, D. H., Hemachandra, L. P., Uusitalo, L. M. & Hempel, N. Bioenergetic analysis of ovarian cancer cell lines: profiling of histological subtypes and identification of a mitochondria-defective cell line. *PloS one* **9**, e98479, doi:10.1371/journal.pone.0098479 (2014).
43 Madar, S., Goldstein, I. & Rotter, V. 'Cancer associated fibroblasts'--more than meets the eye. *Trends Mol Med* **19**, 447-453, doi:10.1016/j.molmed.2013.05.004 (2013).
44 Suh, D. H., Kim, H. S., Kim, B. & Song, Y. S. Metabolic orchestration between cancer cells and tumor microenvironment as a co-evolutionary source of chemoresistance in ovarian cancer: a therapeutic implication. *Biochem Pharmacol* **92**, 43-54, doi:10.1016/j.bcp.2014.08.011 (2014).
45 Joyce, J. A. & Pollard, J. W. Microenvironmental regulation of metastasis. *Nat Rev Cancer* **9**, 239-252, doi:10.1038/nrc2618 (2009).
46 Koontongkaew, S. The tumor microenvironment contribution to development, growth, invasion and metastasis of head and neck squamous cell carcinomas. *J Cancer* **4**, 66-83, doi:10.7150/jca.5112 (2013).
47 Stone, P. J. *et al.* The influence of microvessel density on ovarian carcinogenesis. *Gynecologic oncology* **90**, 566-571 (2003).
48 Alvero, A. B. *et al.* Stem-like ovarian cancer cells can serve as tumor vascular progenitors. *Stem Cells* **27**, 2405-2413, doi:10.1002/stem.191 (2009).
49 Naora, H. Heterotypic cellular interactions in the ovarian tumor microenvironment: biological significance and therapeutic implications. *Front Oncol* **4**, 18, doi:10.3389/fonc.2014.00018 (2014).
50 Schauer, I. G., Sood, A. K., Mok, S. & Liu, J. Cancer-associated fibroblasts and their putative role in potentiating the initiation and development of epithelial ovarian cancer. *Neoplasia* **13**, 393-405 (2011).
51 Zhang, Y. *et al.* Ovarian cancer-associated fibroblasts contribute to epithelial ovarian carcinoma metastasis by promoting angiogenesis, lymphangiogenesis and tumor cell invasion. *Cancer Lett* **303**, 47-55, doi:10.1016/j.canlet.2011.01.011 (2011).
52 Mitchell, J. B. *et al.* Immunophenotype of human adipose-derived cells: temporal changes in stromal-associated and stem cell-associated markers. *Stem Cells* **24**, 376-385, doi:10.1634/stemcells.2005-0234 (2006).
53 Zuk, P. A. *et al.* Human adipose tissue is a source of multipotent stem cells. *Mol Biol Cell* **13**, 4279-4295, doi:10.1091/mbc.E02-02-0105 (2002).
54 Cohen, C. A., Shea, A. A., Heffron, C. L., Schmelz, E. M. & Roberts, P. C. The parity-associated microenvironmental niche in the omental fat band is refractory to ovarian cancer metastasis. *Cancer Prev Res (Phila)* **6**, 1182-1193, doi:10.1158/1940-6207.CAPR-13-0227 (2013).
55 Shea, A. A. *The Impact of Adipose-Associated Stromal Cells on the Metastatic Potential of Ovarian Cancer.*, Virginia Tech, (2014).
56 Yu, G. *et al.* Isolation of murine adipose-derived stem cells. *Methods Mol Biol* **702**, 29-36, doi:10.1007/978-1-61737-960-4_3 (2011).
57 Gerencser, A. A. *et al.* Quantitative microplate-based respirometry with correction for oxygen diffusion. *Anal Chem* **81**, 6868-6878, doi:10.1021/ac900881z (2009).
58 Nerlich, A. G. *et al.* Expression of glutamine:fructose-6-phosphate amidotransferase in human tissues: evidence for high variability and distinct regulation in diabetes. *Diabetes* **47**, 170-178 (1998).
59 Dong, G. *et al.* PKM2 and cancer: The function of PKM2 beyond glycolysis. *Oncol Lett* **11**, 1980-1986, doi:10.3892/ol.2016.4168 (2016).
60 Lee, D. *et al.* Expression of fatty acid binding protein 4 is involved in the cell growth of oral squamous cell carcinoma. *Oncology reports* **31**, 1116-1120, doi:10.3892/or.2014.2975 (2014).
61 Herzog, T. J. Recurrent ovarian cancer: how important is it to treat to disease progression? *Clinical cancer research : an official journal of the American Association for Cancer Research* **10**, 7439-7449, doi:10.1158/1078-0432.CCR-04-0683 (2004).

62 Plecita-Hlavata, L., Lessard, M., Santorova, J., Bewersdorf, J. & Jezek, P. Mitochondrial oxidative phosphorylation and energetic status are reflected by morphology of mitochondrial network in INS-1E and HEP-G2 cells viewed by 4Pi microscopy. *Biochimica et biophysica acta* **1777**, 834-846, doi:10.1016/j.bbabio.2008.04.002 (2008).
63 Malka, F. *et al.* Separate fusion of outer and inner mitochondrial membranes. *EMBO Rep* **6**, 853-859, doi:10.1038/sj.embor.7400488 (2005).
64 Pletjushkina, O. Y. *et al.* Effect of oxidative stress on dynamics of mitochondrial reticulum. *Biochimica et biophysica acta* **1757**, 518-524, doi:10.1016/j.bbabio.2006.03.018 (2006).
65 Ishihara, N., Fujita, Y., Oka, T. & Mihara, K. Regulation of mitochondrial morphology through proteolytic cleavage of OPA1. *EMBO J* **25**, 2966-2977, doi:10.1038/sj.emboj.7601184 (2006).